Evaluation of field sand liquefaction including partial drainage under low and high overburden using a generalized bounding surface model

El-Sekelly, W.[1]*, Dobry, R.[2], Abdoun, T.[3], and Ni, M.[4]

[1]Associate Professor, Dept. of Structural Eng., Mansoura University, Mansoura, Egypt and Research Scientist at New York University Abu Dhabi, Abu Dhabi, United Arab Emirates, email: welsekelly@mans.edu.eg (* corresponding author)

[2] Emeritus Professor, Dept. of Civil and Environmental Eng., Rensselaer Polytechnic Institute, 23 Mann Boulevard, Clifton Park, NY 12065, email: dobryr@rpi.edu

[3] Iovino Chair Professor, Dept. of Civil and Environmental Eng., Rensselaer Polytechnic Institute, 110 8th Street, JEC 4049, Troy, NY 12180 and Global Distinguish Professor, New York University Abu Dhabi, P.O.Box 129188 Abu Dhabi, UAE, email: abdout@rpi.edu

[4] Software development engineer at Amazon Development Center, P. O. Box 81226 Seattle, WA, 98105, email : niminly2008@gmail.com

Abstract

The article presents simulations of the seismic liquefaction response of dense and loose clean Ottawa sand under low and high overburden in the centrifuge, using Program FLAC3D and the P2Psand constitutive model. P2Psand was initially calibrated with cyclic stress-controlled triaxial tests and then modified with information from two centrifuge experiments. The calibrated model was used to simulate four centrifuge tests covering relative densities from 45% to 80% and overburden pressures from about 100 kPa (1 atm) to 600 kPa (6 atm). The four numerical computations were fully coupled effective stress simulations that allowed for pore water pressure buildup and dissipation at every time step. The calibration yielded very good matches between numerical and experimental results in all four centrifuge experiments, and calibrated P2Psand input parameters are suggested for practitioners in similar clean sands. The simulations confirmed the increased diffusivity of the sand layer under high overburden obtained before from the centrifuge results. The reason is that P2Psand assumes that the sand bulk modulus is proportional to the square root of the mean effective stress, consistent with the similar conclusion derived from the centrifuge data. The calibrated P2Psand model was also used to perform "no flow" simulations of the same four centrifuge experiments, in which fluid flow was not allowed during or after shaking. No flow simulations are used sometimes in practice to reduce numerical effort, on the assumption that liquefaction in the field is mostly undrained. It was found that this assumption may produce useful engineering results for a low overburden of 1 atm, but it may become increasingly incorrect and too conservative at higher overburden. The reason is that for certain field conditions, fluid flow becomes more significant during shaking under high overburden due to increased sand diffusivity.

Keywords

Sand liquefaction, constitutive modeling, bounding surface, centrifuge experiments

1. Introduction and literature review

Liquefaction of soils can have devastating consequences to structures and soil-structural systems. Structures and dams that are located on soils that liquefy can be severely damaged during earthquakes resulting in huge loss of lives and assets. Traditionally, the liquefaction potential has been estimated using the Simplified Procedure, originally developed by Seed and Idriss (1971). In this method, the earthquake demand is estimated using the Cyclic Stress Ratio, CSR – related to the seismic shear stress acting on the soil - while the site resistance is estimated with the Cyclic Resistance Ratio, CRR. Both CSR and CRR are evaluated neglecting any stress-strain softening at the site due to the pore pressure buildup in any layer including the critical layer (Youd et al., 2001; Idriss and Boulanger, 2008). Liquefaction is predicted if CSR > CRR. The CRR has been correlated to several field measurements: such the Standard Penetration Test (SPT), the Cone Penetration Test (CPT) and the shear wave velocity (V_s). In practice, liquefaction charts linked to these field measurements are used based on the Simplified Procedure, with these charts calibrated by field case histories of liquefaction and no liquefaction during earthquakes.

Most of these available case histories correspond to effective vertical overburden pressures on the critical liquefiable layer, σ'_{v0} of less than 1 atm, and none of them exceeding 2 atm (Andrus and Stokoe, 2000; Kayen et al., 2013 and Boulanger and Idriss, 2014). Therefore, they are clearly valid at representative overburden pressures of about 1 atm; in fact, some liquefaction charts have been explicitly developed for 1 atm by appropriate normalization of the case histories (Idriss and Boulanger, 2008). However, in the case of tall embankment dams, for example, the liquefiable sand layer in the foundation soil may be subjected to σ'_{v0} much greater than 1 or 2 atm; up to or even higher than 10 atm (Gillette, 2013). In the absence of case histories during actual earthquakes at these high pressures, Seed (1983) proposed the use of an overburden pressure correction factor (K_σ), valid for $\sigma'_{v0} > 1$ atm. Undrained cyclic stress-controlled triaxial or simple shear tests at both 1 atm as well as at the high $\sigma'_{v0} > 1$ atm, are conducted in order to generate the $K_\sigma = (CRR)_{\sigma'v0} / (CRR)_1$, where $(CRR)_{\sigma'v0}$ and $(CRR)_1$ are the cyclic resistance ratios at σ'_{v0} and 1 atm, respectively. These undrained tests invariably produce $K_\sigma < 1.0$ for overburden pressures greater than 1 atm. As a result, the current state of practice always recommends values of $K_\sigma < 1.0$ at high overburden pressures (Seed and Harder, 1990; Vaid and Thomas, 1995; Hynes et al., 1999; Youd et al., 2001; Boulanger, 2003; Boulanger and Idriss, 2004; Idriss and Boulanger, 2006; 2008; Montgomery et al., 2012 ; Dobry and Abdoun, 2015).

Ni et al. (2020) conducted two pairs of liquefaction centrifuge experiments simulating idealized field conditions at $\sigma'_{v0} = 100$ and 600 kPa (1 and 6 atm) listed in Table 1, and obtained $K_\sigma > 1.0$, in contradiction with the State of Practice, where invariably $K_\sigma < 1.0$. They attributed the discrepancy to partial drainage in the critical sand layer during shaking in the centrifuge, with this drainage being more pronounced at 600 kPa (6 atm). This partial drainage is completely prevented in the undrained cyclic tests that serve as the basis for K_σ values in the current State of Practice. Ni et al. (2020) and Abdoun et al. (2020) further concluded that the increased volumetric drained stiffness of the sand at 6 atm was responsible for this more significant drainage. Abdoun et al. (2020) recommended additional experimental and numerical work in order to understand better liquefaction response at high confining pressure. This paper is focused on such numerical simulation of the sand layer under low and high overburden pressure in the four centrifuge tests reported by Ni et al. (2020).

During the last few decades, researchers have developed a number of numerical models that aim at capturing the liquefaction response of sands to liquefaction-inducing cyclic shearing

(Prevost, 1977; Li et al., 1993; Mckenna and Fenves, 2001; Elgamal et al., 2003; Dafalias and Manzari, 2004; Gerolymos and Gazetas, 2005; Boulanger and Ziotopoulou, 2013; Wang et al. 2014; Barrero et al., 2019; Zou et al., 2020). Some of these material models have been implemented in commercial finite elements and finite difference software. FLAC3D (Fast Lagrangian Analysis of Continua in 3 Dimensions) is a popular finite difference commercial code, commonly used in practice in soil-structure problems, particularly those which involve dynamic excitation and liquefaction. FLAC3D has recently included its in-house liquefaction constitutive model for sands, named P2Psand (Cheng, 2018; Cheng and Detournay, 2021), that builds on the bounding surface model originally developed by Dafalias and Manzari (2004)

The purpose of the paper is to implement the recent P2Psand numerical model to understand the liquefaction behavior of sand in the idealized field conditions of the centrifuge, under low and high overburden. It aims at determining a set of input parameters that may be used by practitioners in similar sands for a range of confining pressures and relative densities.

The P2Psand model was calibrated in four main steps: (i) initial calibration using available cyclic stress controlled triaxial results on dense soil of the same clean Ottawa F65 sand of the centrifuge tests, published by Liquefaction Experiments and Analysis Projects, LEAP (Manzari et al., 2017); (ii) comparison between FLAC3D predictions using this calibration, and the pore pressures measured in one of the centrifuge tests on dense sand of Table 1; (iii) adjustment of the calibration to account for centrifuge-specific information including those centrifuge pore pressures measured in dense sand; and (iv) adjustment of the sand contraction parameter for the simulation of one of the centrifuge tests on loose sand of Table 1, using cyclic triaxial data presented by Vaid and Sivathayalan (1996) and reported by Idriss and Boulanger (2008).

The calibrated model was then used to simulate the four centrifuge experiments listed in Table 1, covering for the critical liquefiable sand layer relative densities of 45% and 80%, and effective overburden pressures of 100 and 600 kPa (1 and 6 atm). Since the results of the centrifuge experiments were available during the numerical simulation, they are considered Class C simulations of the centrifuge experiments as defined by VELACS (Arulanandan and Scott, 1993), as well as by ongoing project LEAP (Manzari et al., 2017). The numerical simulations were fully coupled with pore pressure build up and fluid flow and dissipation being updated at every time step.

The paper starts with a summary of the centrifuge tests listed in Table 1, with focus on the measured results to be simulated by FLAC3D. Details of this experimental work are published elsewhere (Ni et al., 2020, Abdoun et al., 2020). A brief description of the P2Psand model is then presented along with the FLAC3D model setup. A detailed description of the P2Psand calibration process adopted by the authors is presented, including the changes in the main parameters from their default values, followed by a comparison between measured and simulated centrifuge results. A section is dedicated to the fluid flow (diffusivity) characteristics of the layer. Diffusivity plays a critical role in conjunction with the drainage boundaries, in the degree of partial drainage during shaking as well as in the rate of pore pressure dissipation after shaking. This is true at both low and high overburden pressures. Following this, simplified "no flow" numerical simulations -that do not allow for fluid drainage- were performed and compared to the fully coupled simulations and experimental results. This was done in order to assess the accuracy and relevance of the undrained simplification that is sometimes used in practice to reduce computational effort, including high overburden pressure simulations (Gillette, 2021).

2. Summary of experimental work

The four centrifuge experiments listed in Table 1 were performed using the lightweight aluminum laminar container and shaking table in the geotechnical centrifuge facility at Rensselaer Polytechnic Institute (RPI). All experiments were conducted on an approximately 5 m layer of saturated clean Ottawa F65 sand having an impervious boundary at the bottom and a free drainage boundary at the top. Characteristics and grain size distribution of this sand have been reported elsewhere (El Ghoraiby et al., 2017; Manzari et al., 2017). All dimensions mentioned in this paper are in prototype units unless stated otherwise. Two of the centrifuge experiments were performed at a relative density, D_r of about 45% (Tests 45-1 and 45-6) while the other two were performed at D_r of about 80% (Test 80-1 and 80-6). The average vertical effective stress in the sand layer was about 1 atm (~100 kPa) in Tests 45-1 and 80-1, and about 6 atm (~600 kPa) in Tests 45-6 and 80-6. The two setups used for the centrifuge models are shown in Fig. 1. In all cases, they represent a dry pluviated saturated clean sand layer about 5 m thick, covered by a dry lead shot layer of variable thickness. The lead shot provided the desired vertical effective pressure, as well as the right level of inertially-generated horizontal shear stresses during shaking in the sand. In order to prevent the lead shot from sinking into the saturated sand, a transition filter layer was added in between. The dry pluviated sand was saturated with a viscous fluid of appropriate viscosity depending on the g level, in order to maintain the fluid flow characteristics of the sand at 1 g. Additional details about the construction and saturation procedure of the model can be found in Ni et al. (2020). Each model was subjected to sinusoidal excitation at the base, having the right acceleration level designed to generate in the sand a maximum pore pressure ratio, $(r_u)_{max} = (u/\sigma'_{v0})_{max} \approx 0.8$, where u = excess pore pressure.. This target pore pressure ratio of 0.8, while close enough to the full liquefaction condition of $(r_u)_{max} \approx 1.0$ to allow for the desired evaluation of soil liquefaction resistance at low and high σ'_{v0}, is enough below full liquefaction to avoid phenomena like particle flotation and resettlement, which would have added challenges and uncertainties to the numerical modeling (Scott, 1986; Sharp and Dobry, 2002)

Figures 2 and 3 display the measured time histories of excess pore pressure ratio during and after shaking in the four tests, as reported by Ni et al. (2020). While the target maximum excess pore pressure ratio, $(r_u)_{max}$ was 0.8, Table 1 shows that the measured $(r_u)_{max}$ were generally somewhat different from 0.8. The actual measured pore pressure ratios were used in all analyses and discussions presented herein. Figures 2 and 3 indicate three things: (i) $(r_u)_{max}$ was invariably reached at the end of shaking (~5 seconds), near the bottom of the layer where the impervious boundary is located; (ii) the values of r_u were smaller at shallower depths, especially near the top where the pervious boundary is located, indicating partial drainage during the shaking; and (iii) the degree of partial drainage and correspondingly lower values of r_u at shallower elevations were much more pronounced in the 6 atm tests compared to the 1 atm tests.

Figures 4 and 5 show the time histories of acceleration during shaking, measured at different depths in the same four centrifuge tests. The input acceleration consisted of a 10-cycle uniform sinusoidal motion having a prototype frequency of 2 Hz. In order to reach a target maximum pore pressure ratio of about 0.8 in all the tests, the input acceleration amplitude had to be almost an order of magnitude higher at 6 atm compared to the 1 atm tests.

Figures 6 and 7 show the time histories during shaking of the stress ratio (shear stress (τ) / σ'_{v0}), at different depths in the four tests. Ni et al. (2020) used the System Identification technique developed by Elgamal et al. (1995, 1996) and Zeghal et al. (1995), to obtain these shear stresses at multiple elevations from the acceleration recordings.

Finally, Figs. 8 and 9 present the time histories of vertical strain at the surface of the sand layer, while Figs. 10 and 11 show the time histories of the same surface vertical strain starting after the end of shaking, measured in the same four centrifuge tests, as reported by Ni et al. (2020). The vertical strain equals (S/H)*100, where S is the settlement of the layer measured using the LVDT placed at the sand layer surface (Fig. 1), and H is the thickness of the deposit.

Further discussion of these experimental data is presented later in the paper along with the corresponding results from the numerical simulations.

3. Numerical analysis

3.1.Material model description

All analyses presented in this paper were performed using the P2Psand (Practical Two-surface Plastic Sand) constitutive model. This model was developed by Cheng (2018) and Cheng and Detournay (2021) for dynamic and earthquake engineering applications in sand. It is a modification of fabric-dilatancy related sand plasticity DM04 model proposed by Dafalias and Manzari (2004). Cheng and Detournay (2021) showed that the modified version has improved performance and reduced complexity compared to the original DM04 model. P2PSand maintains the bounding surface plasticity framework originally included by Manzari and Dafalias (1997) and Dafalias and Manzari (2004). It uses relative density instead of void ratio for defining the state parameter, as shown in Cheng and Detournay (2021). P2PSand is designed to use the same general model constants for a wide range of initial relative densities and initial stress states. The details of the material model formulation can be found in Cheng and Detournay (2021). Table 2 lists the user defined parameters in the P2PSand model, describes each parameter and – when available – provides the corresponding expression used to calculate the default value. As can be noted from the table, the user is allowed to change as many as twenty parameters. Since P2Psand aims at being user friendly to practitioners, most of the parameters have a default value recommended by the model developers (Cheng and Detournay, 2021). In fact, it is possible for the user to input only the relative density or an equivalent index parameter for the sand, obtained from the SPT blow count or CPT tip resistance. Table 2 lists the values of all default parameters evaluated at a relative density, $D_r^0 = 71.5\%$ - labeled Set A in the table - which defines the starting point for the calibration conducted in this paper.

3.2. FLAC3D model setup

The numerical platform used herein is FLAC3D version 7. FLAC3D is a three dimensional numerical modeling software that utilizes an explicit finite volume formulation in an explicit, Lagrangian calculation scheme and the mixed-discretization zoning technique. It is commonly used by geotechnical engineers in practice for geotechnical analyses of soil, rock, groundwater, and ground support systems. The dynamic analysis feature was utilized in the simulations presented in this paper. The analyses were performed in the time domain and are characterized by being fully coupled non-linear path-dependent. Different materials are represented in FLAC3D by elements or zones connected together with grid points or nodes.

The centrifuge tests simulations were performed at the prototype scale (Fig. 1). The numerical model was built using 8-nodes brick zones stacked on each other and connected at the nodes to form the corresponding soil column shown in Figure 1. The numerical grid consisted of a uniform layer of sand overlaid by a transition layer which had on top of it a layer of lead shot, one zone wide and 11 to 20 zones high depending on the experiment simulated. The aspect ratio was maintained as close to 1:1 as possible with a maximum of 2:1. The numerical model was meant to simulate a single soil column rather than the full experimental model. An elastic analysis using the Mohr-Coulomb material model was first conducted with appropriate stress-dependent stiffness to establish the initial geostatic conditions of the soil column before shaking. In this initial phase, the Poisson's ratio was adjusted to generate a lateral earth pressure coefficient at rest, $K_0 \approx 0.5$. The boundary conditions were fixed at the base, with only vertical motions allowed in the soil column assuming a frictionless wall, which is a realistic assumption given that the soil was placed inside a very low friction latex membrane within the laminar container. As explained before in Section 2 and illustrated in Fig. 1, the centrifuge tests were performed in this laminar container having flexible walls, which approximated a shear beam horizontal dynamic response. In order to accurately capture this behavior in the numerical analysis, each node was linked to all nodes at the same elevation in order to move together as a shear beam. A saturation value of 1.0 was maintained in both the sand and transition layer to simulate the experimental condition where the water table was at the top of the transition layer.

Once the initial geostatic conditions were established, the sand was assigned the P2Psand constitutive model and the soil was allowed to reach equilibrium again. After that, the dynamic phase started with the soil column being fixed at the base and free to move elsewhere, still maintaining the shear beam behavior. The corresponding sinusoidal base motion was then applied at the base of the soil column, similar to what actually happened in the centrifuge experiments. During both this dynamic phase of the analysis and the dissipation phase after shaking, the fluid flow feature was turned on to allow for fully coupled effective stress analysis. The hydraulic boundary conditions were similar to that of the centrifuge: impervious side and base boundaries and pervious top boundary. A permeability value of 0.001-0.0012 m/sec (depending on the sand relative density) was assigned to the sand layer, as measured in LEAP (2017). The maximum time step allowed in the analysis was 1.25E-4 sec in order to ensure adequate solution stability. However, FLAC3D adjusted the actual time step to a much lower value in order to maintain the required accuracy. A small Rayleigh damping was set to 0.5% with a center frequency of 2 Hz.

3.3.Model Calibration

The calibration process was based initially on cyclic triaxial (CTX) undrained stress-controlled results available from the LEAP (2017) database. All existing CTX information in this database corresponds to dense and very dense soils. The most relevant are the results of a series of stress controlled CTXs on Ottawa F65 sand of $D_r = 71.5\%$ under an isotropic effective pressure of 100 kPa (~1 atm). This density and confining pressure are close to the conditions of our centrifuge Test 80-1 (Table 1) – $D_r = 77\%$ and effective overburden pressure of 1 atm - performed using the same Ottawa F65 sand. The corresponding liquefaction strength curve (LSC) for the LEAP cyclic triaxial tests is included in Fig. 12a.

This initial calibration - based on the experimental LSC of Fig. 12a - was then adjusted to incorporate information obtained from our dense sand centrifuge Test 80-1. The centrifuge information from Test 80-1 used for the adjustment included the actual relative density and shear wave velocity of the sand measured in the centrifuge experiment, as well as the pore pressures measured in the sand during and after shaking. Finally, the calibration was extended to the loose sand of $D_r = 45\%$, by incorporating information from cyclic triaxial testing data at different densities reported by Idriss and Boulanger (2008). In this last step, only the factor-cyclic K_c was modified to account for the change of density from 71.5% to 45%, with the value of Elasticity-r G_r determined from the bender element shear wave velocity measurements in Test 45-1.

The evolution of the calibration process for $D_r \approx 70\text{-}80\%$ may best be followed with the help of input parameter Sets A through D in Table 2, where Set A contains the default parameters associated with the $D_r^0 = 71.5\%$ of the sand in the cyclic triaxial results of Fig. 12a, and Set D corresponds to the parameters finally adopted in this paper for the FLAC3D centrifuge simulations on dense sand of $D_r = 77\%$. The modified Set D parameters for $D_r = 45\%$ are included in Table 3. Additional detail on the calibration is provided in the next paragraphs.

The process started by simulating with FLAC3D the LSC from LEAP in Fig. 12a, using the default parameters provided in the P2Psand model for an initial sand relative density, $D_r^0 = 71.5\%$, which is the actual density used in these triaxial tests (Set A in Table 2). It must be noted that in this Set A (along with Sets B, C and D), the actual maximum ($e_{max} = 0.78$) and minimum ($e_{min} = 0.51$) void ratios rather than the default values were used, with these measured void ratios obtained from LEAP (2017). The simulated cyclic triaxial LSC curve using P2Psand and Set A has been included in Fig. 12a, where it plots significantly higher than the experimental LEAP LSC.

The next step was to change only the parameter that controls the rate of sand contraction (known as factor-cyclic, K_c), while not changing any of the other seventeen default parameters associated with $D_r^0 = 71.5\%$. The default $K_c = 0.1857$ was increased in an effort to move the simulated LSC downwards toward the experimental LSC. Several values of K_c were tried up to $K_c = 2$, shown in Fig. 12b (Set B in Table 2). While the simulated LSC has indeed moved downwards, the slope of this numerical LSC with $K_c = 2$ in Fig. 12b has also become much steeper than that of the experimental curve.

This difference in slope between simulated and experimental triaxial curves in Fig. 12b triggered the need to modify other parameters away from their default values, in addition to K_c, in order to match the experimental LEAP triaxial LSC as closely as possible. Several trials were performed, with the best match shown in Fig. 12c, and with the corresponding parameters listed in Table 2 (Set C). In this Set C, three out of a total of seventeen parameters associated with $D_r^0 = 71.5\%$, were changed, with the other fourteen maintaining their default values, as shown in Table

2. The three parameters changed from Set A to Set C at $D_r^0 = 71.5\%$ were: K_c (0.1857 to 0.3); n^d = (0.465 to 1); and h_0 (1.7 to 0.5).

Set C – obtained using exclusively the LEAP cyclic triaxial tests without reference to our centrifuge results - was then used to model the pore pressure response of centrifuge Test 80-1, with the results shown in Fig. 13 in black dashed lines. As this simulation did not consider any measured data from the centrifuge tests listed in Table 1, it is a Class B simulation as defined by VELACS (Arulanandan and Scott, 1993), as well as by ongoing project LEAP (Manzari et al., 2017). The match in Fig. 13 between the experimental Test 80-1 and its numerical simulation using Set C is poor, with the measured pore pressures underpredicted at all depths.

In order to reach a better match between numerical and experimental simulations for centrifuge Test 80-1, Set C was adjusted in a final step to a new set of parameters (Set D in Table 2). Two types of adjustments were implemented: (i) change from the $D_r^0 = 71.5\%$ of the cyclic triaxial tests to the $D_r^0 = 77\%$ of centrifuge Test 80-1, and replacement of $G_r = 967.2$ by $G_r = 772$ corresponding to the shear wave velocity measured in the sand by bender elements in the same centrifuge test; and (ii) slight change in other four parameters. The change in these four parameters was conducted in order to improve the comparison with the centrifuge results, while simultaneously preserving the good match with the LEAP LSC curve achieved before in Fig. 12c using Set C. These other four parameters slightly changed between Sets C and D were: K_c (0.3 to 0.32); Q (10 to 9); h_0 (0.5 to 0.4); and ν (0.14 to 0.1). The change in the Poisson's ratio ν took into account the need to improve the simulation of the measured pore water pressure dissipation with time after shaking in centrifuge Test 80-1, as illustrated by Fig. 13 and explained later in more detail in Section 4.5.

The centrifuge pore pressure simulation of Test 80-1 using Set D is shown in Fig. 13 in red dashed lines, where it is now in excellent agreement with the measurements. The simulated LSC using Set D is also compared with the experimental LSC in Fig. 12d, with a very reasonable match, especially at a cyclic stress ratio, CSR of about 0.2 and number of cycles of about 10, which are close to the experimental conditions during shaking of centrifuge Test 80-1.

Figure 14 compares the experimental and numerical stress paths and shear stress-strain loops for the cyclic triaxial test located at the intersection point between numerical and experimental LSC in Fig. 12d. The plots indicate a very good match in terms of stress path, particularly before the onset of liquefaction. Both the simulated and experimental stress paths in Figs. 14a and 14c show signs of dilation followed by increased contraction at an average effective confining pressure, P of about 50 kPa. The comparison of shear stress-strain loops in Figs. 14b and 14d is also reasonably good.

In order to simulate the two centrifuge tests of Table 1 with sand at a relative density of 45%, three parameters were adjusted from the Set D listed in Table 2:

- The "relative-density-initial, D_r^0 " which defines the initial relative density of the sand before seismic shaking (from 77% to 45%).
- The "elasticity-r, G_r" which defines the modulus of elasticity of the sand deposit. This information was obtained from the shear wave velocity measured in centrifuge Tests 45-1 and 45-6 using bender elements (from 772 to 596).
- The "factor-cyclic, K_c" which defines the rate of contraction and cyclic mobility. The LEAP database does not include any cyclic triaxial test data at relative densities close to 45%. Therefore, it was decided to adjust K_c using data from the stress controlled cyclic

triaxial tests on clean Fraser Delta sand, conducted at a consolidation pressure of 100 kPa and using several relative densities, performed by Vaid and Sivathayalan (1996) and reported by Idriss and Boulanger (2008). Figure 15 plots the measured cyclic strength versus relative density for these tests. The cyclic shear strengths for relative densities of 45% and 71.5% were found by interpolation to be about 15 and 27 kPa, as shown in the figure. The ratio between these two values of cyclic strength (15/27 = 0.56) was then used to plot in Fig. 16, an "experimental" cyclic triaxial LSC that represents the loose Ottawa F65 sand (D_r = 45%), by just shifting down by this factor 0.56, the actual experimental LSC curve for Ottawa sand at 100 kPa reported by LEAP (2017) and plotted in Figs. 12a through d. This new "experimental" curve is labeled "Interpolated Exp. CTX 1 atm D_r = 45%" in Fig. 16. The factor-cyclic, K_c was then adjusted in an iterative process using FLAC3D simulations of these CTX tests, until the simulation matched well in Fig. 16 the "experimental" LSC for D_r = 45% at around ten cycles of loading with a K_c value of 0.8. This value of K_c = 0.8 – included in Table 3 for D_r = 45% - was also found to yield a very good match between experimental and numerical excess pore pressure measured in the corresponding centrifuge Test 45-1 (Fig. 2a).

<u>Additional verification:</u> As explained above, the calibration was entirely performed for a level of confinement of about 100 kPa (1 atm), based on available cyclic triaxial data on sand conducted with an isotropic consolidated pressure of 100 kPa, and refined with results from the two centrifuge experiments that used an overburden pressure of 1 atm (Tests 80-1 and 45-1). In order to further verify the general validity of the calibrated parameters of Table 3 at the higher pressure of 600 kPa (6 atm), the experimental LEAP LSC at 100 kPa plotted in Figs. 12a through d was adjusted for confining pressure using the commonly used overburden correction factor, K_σ, proposed by Idriss

and Boulanger (2008). This K_σ at 600 kPa (6 atm) is equal to 0.73 and 0.84 for relative densities of 71.5% and 45%, respectively. These factors were used to generate two "K_σ- predicted" LSCs for relative densities of 71.5% and 45% and a confining pressure of 600 kPa (6 atm) in Figs. 12d and 16, respectively. The same figures also present the LSCs of simulated CTX subjected to a confining pressure of 600 kPa (6 atm) using FLAC3D and P2Psand with the parameters listed in Table 3. Figures 12d and 16 show a reasonable match between these simulated and the "K_σ-predicted" LSCs at 6 atm. While it would be possible to adjust the model parameters to reach a better match, this would completely defeat the philosophy of the model, which should be the same for different levels of confining pressure. Moreover, maintaining the same parameters at 1 and 6 atm in the numerical simulations of the actual centrifuge tests, yielded also a very good match for the two different overburden pressures used in the centrifuge tests, as shown in Figs. 2 and 3.

4. Numerical Fully Coupled Results

The FLAC3D simulations of the four centrifuge tests of Table 1, presented below, used P2Psand with the Set D parameters listed in Table 3.

4.1.Pore pressure histories

Figures 2 and 3 show the computed time histories of excess pore pressure ratio, predicted by FLAC Runs 45-1, 45-6, 80-1, and 80-6, and compare them with the corresponding centrifuge experimental results. Both the rates of buildup and dissipation match very well in most cases between measured and computed excess pore pressures. The only exception is the measured excess pore pressure in the middle of the sand layer in Test 45-1, where the numerically computed buildup rate and total accumulated excess pore pressure are smaller than the measured ones. It is not clear to the authors whether this discrepancy was caused by an experimental or a numerical issue. In the numerical model, the buildup rate is mostly determined by the “factor-cyclic K_c” which influences the rate of cyclic mobility and liquefaction (contraction). The dissipation rate is in turn controlled by the Poisson’s ratio, v, already mentioned and further discussed later herein. The figures show that dissipation after shaking is much faster at 6 atm than at 1 atm, in both actual and simulated centrifuge experiments. It must be noted that the value of K_c is solely dependent on relative density. The lower the relative density, the higher the contractive tendency of the sand. For the same relative density, the K_c as well as ALL the rest of the parameters are the same in Table 3 irrespective of effective overburden pressure. The effect of confining pressure on the contractive tendency of the soil is inherently included in the formulation of the model (Cheng and Detournay, 2021). Figures 2 and 3 also show that the numerical simulations do not capture the transient response (cyclic component) of the measured pore pressure histories. This transient behavior in the measured pore pressure histories are mostly due to the sensor motion during shaking, and hence is not associated with the actual response of the soil to the horizontal excitation.

4.2.<u>Acceleration histories</u>

Figures 4 and 5 show the computed time histories of acceleration at different depths, recorded in Flac3D runs 45-1, 45-6, 80-1, and 80-6, and compare them to the corresponding experimental results. The input acceleration consisted of a 10-cycle uniform sinusoidal motion having a prototype frequency of 2 Hz. The comparisons range from fair to very good. The best comparisons correspond to the bottom elevation, and more generally to the first few cycles before the effect of generated excess pore pressure kicks in. This is especially clear in the comparison between Test 45-1 and Flac 45-1, where the experimental acceleration in the middle and top of the layer degrades rapidly, while the computed acceleration degrades very little. This is probably associated with the lower numerical excess pore pressure ratio in the middle of the sand layer in Test 45-1 (Figure 2).

Except for this problem in the middle and top of the layer for Flac 45-1 in Fig. 4, the rest of the comparisons at the bottom layer in this test, as well as the other three tests at all elevations and throughout the shaking, are generally good to very good.

4.3. <u>Shear stress histories</u>

Figures 6 and 7 show the time histories of shear stress ratios, computed in numerical Flac runs 45-1, 45-6, 80-1, and 80-6. The figures compare these computed histories to the measured histories. The graphs show a very good match for the stress histories, especially during the first few cycles before the effect of excess pore pressure kicks in. As the experimental stress ratios were obtained from the acceleration time histories of Figs. 4 and 5 using System Identification, it should be expected that the stress ratio comparisons should exhibit similar features to those just described for the acceleration time histories. This is what happens in Fig. 6, with only fair agreement in Flac 45-1 after the first few cycles. On the other hand, the agreement for the other three Flac simulations at all elevations and times is uniformly excellent.

4.4. <u>Settlement</u>

Figures 8 and 9 show the time histories of vertical strain, while Figs. 10 and 11 show the time histories of vertical strain after the end of shaking, computed in numerical Flac runs 45-1, 45-6, 80-1, and 80-6. The graphs compare the computed vertical strains to the measured ones. The vertical strain equals (S/H)*100, where S is the settlement measured using the vertical LVDT atop of the layer, and H is the layer thickness. Figures 8 and 9 showing the total settlement from beginning of shaking reveal that:

- The computed settlement is generally smaller than the experimental settlement, with the exception of Test 80-6.

- The cyclic component of the settlement history only appears in the measured but not the computed settlement. The cyclic component of the measured settlement is probably due to the cyclic motion of the LVDT or its mounting brackets.

Figures 10 and 11 -presenting the settlement after the end of shaking- show excellent matches between computed and measured settlement at 1 atm (Test 45-1 and Test 80-1). This is probably associated with the fact that settlement after the end of shaking is mostly due to consolidation, which is well suited to the capabilities of the numerical model. The comparisons at 6 atm show some discrepancies, especially for Test 45-6 where the computed values are about 50% higher than the measured settlements. It is not clear to the authors what is causing this discrepancy. It must be noted that for the 6 atm tests, most of the settlement occurred during shaking, as shown in Figs. 8b and 9b, so the remaining settlement after the end of shaking was very small, possibly resulting in a greater experimental error.

4.5. Coefficient of consolidation and diffusivity

In FLAC3D, the diffusivity, *C,* is calculated from Biot (1955) theory of consolidation, based on the following equation for incompressible grains:

$$C = C_v = \frac{k}{\frac{n}{K_f} + \frac{1}{\alpha_1}} \tag{15}$$

$$\alpha_1 = K + \frac{4}{3} G = \left(\frac{2(1+v)}{3(1-2v)} + \frac{4}{3} \right) G \tag{16}$$

where k is the fluid mobility coefficient (sand permeability divided by the unit weight of water: 1.2 E -5 and 1.0 E-5 m^4/kN.sec for the loose and dense sand used in our centrifuge tests, respectively); n is the porosity (0.4 and 0.35 for loose and dense sand); K_f is the fluid bulk modulus (2.2E-6 kPa); G is the shear modulus; and K is the bulk modulus of the soil, $K =$

$2G\ (1+v)/3(1-2v)$. While in the FLAC3D simulations of the centrifuge tests, k, n, v and K_f remain constant throughout shaking and dissipation, the value of G (and thus also of K) varies as the effective stress changes during excess pore pressure build-up and dissipation. The influence of the effective stress change due to the evolution of the excess pore pressure, is intrinsically handled by P2PSand through the change in G, by the fact that G ~ $\sqrt{\sigma'_0}$, where σ'_0 = mean effective normal stress. The diffusivity, C, in Eq. 15 is identical to the coefficient of consolidation, C_v, used in Terzaghi's theory of consolidation (Terzaghi et al. 1996). All variables in Eqs. 15 and 16 were measured or estimated experimentally for the Ottawa F65 sand used in the centrifuge tests (LEAP 2017, El Ghoraiby et al. 2017 and Ni et al. 2020), except for the Poisson's ratio v. As mentioned before in Section 3.3, v was adjusted from the default value of 0.14 to 0.1 in order to obtain the correct rate of pore pressure dissipation after shaking measured in centrifuge Test 80-1. Once v was adjusted for the Test 80-1 simulation, it was found that the same v = 0.1 yielded very reasonable results for other three centrifuge simulations.

Equation 15 was used to generate the time history of diffusivity, $C = C_v$, for each centrifuge simulation, based on the values of G and K at each time increment. The four calculated time histories of $C = C_v$ are displayed in Figs. 17 and 18. The graphs show that the diffusivity first decreases with time during shaking (t < 5 seconds), and then increases with time after the end of shaking. The reason is that as the shaking progresses, the increased excess pore pressure results in a reduction in vertical effective stresses, and thus also in a reduction of both shear and bulk moduli, which are dependent on the average effective stress. Afterwards and for t > 5 seconds, the excess pore pressures gradually dissipate, resulting in an increase in the vertical effective stresses and hence increases in the shear and bulk moduli, which translates into increasing diffusivity C. Each of the four plots in Figs. 17 and 18 also include one data point for the value of C_v obtained by

Abdoun et al. (2020) at a specific time instance during dissipation from the measured pore pressure and settlement in the centrifuge tests. Figures 17 and 18 indicate an excellent match between experimental and numerical diffusivity, even though they were based on two different consolidation theories.

Figures 17 and 18 also show that the diffusivity at 6 atm is about three times higher than that at 1 atm (3 to 4 m^2/s versus 1 to 1.5 m^2/s), which explains the much faster dissipation of excess pore pressure at 6 atm already noted in Figs. 2 and 3. This suggests that the excess pore pressures in the sand at 6 atm are draining much faster than at 1 atm, both during and after shaking. This more partial drainage in turn results in less liquefaction vulnerability at a higher vertical overburden pressure.

5. **Numerical no flow simulations**

The results presented in the previous sections of the paper –corresponding to the four FLAC3D runs listed in Table 1– were fully coupled numerical simulations, with fluid flow and partial drainage updated at every time step and allowed at all times during and after shaking. While this is the most rigorous analysis procedure, and a very good match was achieved between experimental and numerical results, sometimes a different approach is used in practice. The reason is that it is computationally expensive and requires relatively precise knowledge about permeability and drained moduli of the sand (Gillette, 2021). Therefore, sometimes a "no flow" analysis is performed in which no water drainage is allowed during shaking, including situations of high overburden pressure. The basic assumption is that this is a good engineering approximation as the liquefaction phenomenon in the field is mostly undrained.

In order to evaluate this practice at low and high overburden pressures, the authors conducted four FLAC3D "no-flow" simulations for the centrifuge Tests 45-1, 45-6, 80-1, and 80-

6, in which fluid flow was turned off during and after shaking. These four runs were otherwise identical to the four FLAC3D runs listed in Table 1, including use of the same acceleration input time histories and P2Psand sand parameters of Table 3.

The results and comparisons for these no flow runs are shown in Figs. 19 and 20. Figure 19 shows the excess pore pressure ratio histories for both fully coupled and no flow numerical simulations and compares both to the experimental results. Figure 20 presents the instantaneous excess pore pressure ratio profiles at the end of shaking at the time, t = 5 sec, which is in all cases equal or very close to the maximum excess pore pressure ratio at each elevation. The two figures reveal that:

- As noticed before herein, the pore pressure ratios of the fully coupled simulations follow closely the experimental results, both versus time and versus depth.
- The pore pressures from the no-flow simulations are also reasonably in agreement with the experimental results during shaking at 1 atm for Tests 45-1 and 80-1. They diverge significantly from both experimental and fully coupled experimental results only after shaking (Fig. 19a and c), where dissipation was not allowed in the "no flow" simulations. As the experimental pore pressures invariably decrease during dissipation, this does not affect the good agreement in Figs. 19a,c and 20a,c in the maximum pore pressure ratios, with all maximum values happening during shaking. This is important, as evaluation of the maximum pore pressure ratio for the layer or at a given depth is often in practice the main purpose of the numerical simulations. This good agreement during shaking in the pore pressure ratios during shaking in Figs. 19 and 20 may justify – for 1 atm – the basic assumption underlying the use of "no flow" simulations in engineering practice.

- On the other hand, the match with the experimentally measured pore pressure ratios ranges from fair to poor for the pore pressure ratios from the "no flow" simulations during shaking at 6 atm for Tests 45-6 and 80-6 in Figs. 19b and d. This is especially true at $D_r = 45\%$ for Test 45-6, for which the no flow simulation overestimated the excess pore pressure generation at some depths and underestimated it at other depths. This is especially troublesome, as in practice liquefaction of looser sands is a greater concern than that of denser sands, due to their potential for greater engineering effects after liquefaction.
- That is, Figs. 19 and 20 indicate that the liquefaction phenomenon during shaking was indeed not far from undrained during shaking at the low overburden pressure of 1 atm, as sometimes assumed in practice. The same figures also show that this assumption ceased to be valid at the higher overburden pressure of 6 atm, due to the effect of drainage which made the liquefaction phenomenon partially drained rather than fully undrained during shaking. As already discussed herein, this increased partial drainage occurs because of the increased drained modulus and coefficient of consolidation (diffusivity) of the sand as the overburden pressure increases. Therefore, the discrepancy between fully coupled and experimental pore pressures on the one hand, and no flow pore pressures on the other, revealed by Figs. 19 and 20 for 6 atm, is expected to become even worse for the higher overburden of interest in some projects, like 10 or 12 atm.
- Therefore, while it may be computationally expensive to run a fully coupled numerical simulation where water flow and drainage are allowed, it seems to be

crucial for capturing the true liquefaction behavior in some field situations involving a high overburden.

6. Conclusions and Recommendations

A practical 3D field liquefaction numerical model (P2Psand) developed by Cheng and Detournay, (2021), was calibrated using an established experimental dataset of undrained cyclic stress-controlled triaxial reported by LEAP (2017) and Idriss and Boulanger (2008) and modified based on centrifuge experimental results. The calibrated model was used to simulate four centrifuge tests under a wide range of overburden pressures (1-6 atm) and relative densities (45-77 %). P2PSand is based on the bounding surface plasticity theory originally implemented in Dafalias and Manzari (2004) soil model. Based on the presented results and analyses, the authors arrived to the following conclusions and recommendations:

- P2Psand together with FLAC3D constitute a practical tool that may be used by practitioners for similar clean sands using the calibration numerical parameters listed in Table 3, covering wide ranges of overburden pressures from 1 to 6 atm and relative densities from 45 % to 77 %. In future practical applications involving different conditions for which cyclic laboratory tests are not available, at least three parameters may have to be changed by the user; the initial relative density D_r^0, the cycling factor K_c, and the elasticity G_r, as follows:
    - The initial relative density D_r^0 may be estimated from field measurements using the Standard Penetration Test (SPT) or Cone Penetration Test (CPT).

- For relative densities between 45% and 77%, the cycling factor K_c and the elasticity G_r may be estimated based on D_r^0 by linear interpolation of the values used herein and reported in Table 3.

- Based on the numerical and experimental diffusivity and dissipation behaviors discussed in the paper, a sand layer will be more partially drained under a high overburden pressure compared with the situation at 1 atm. This is appropriately accounted for in P2PSand, by the square root law dependency on the effective mean stress of the elastic shear modulus and bulk modulus of the sand.
- Based on the previous conclusion and the results of the parallel "no flow" runs conducted by the authors, "no flow" numerical simulations that do not allow for fluid drainage during shaking may be appropriate at a low overburden pressure in the order of 1 atm, but not necessarily at high overburden pressures of 6 atm or 10 atm of interest in some projects.
- Under some circumstances, sand layers in the field may be less prone to liquefaction under high overburden pressure than suggested by the values of the factor $K_\sigma < 1$ in the current State of Practice (SoP). The reason for this discrepancy is that the current SoP relies on undrained small-scale cyclic tests, while the liquefaction process in the field may be affected by partial drainage rather than being fully undrained, with this partial drainage being more significant at high overburden pressures.

Acknowledgments

This research was performed using the FLAC3D demo version provided by Itasca Consulting Group, Inc. The authors would like to thank Dr. Zhao Cheng from FLAC3D support team for his guidance during the course of this research. The research was supported by the National Science

Foundation under Grants No. 1545026 & 1904313 and NYU Abu Dhabi; this support is gratefully acknowledged.

REFERENCES

Abdoun, T., Ni, M., Dobry, R., Zehtab, K., Marr, A., & El-Sekelly, W. (2020) Pore Pressure and K σ Evaluation at High Overburden Pressure under Field Drainage Conditions. II: Additional Interpretation. Journal of Geotechnical and Geoenvironmental Engineering, 146(9), 04020089.

Andrus, R. D., & Stokoe II, K. H. (2000) Liquefaction resistance of soils from shear-wave velocity. Journal of geotechnical and geoenvironmental engineering, 126(11), 1015-1025.

Arulanandan, K., & Scott, R. F. (1993). Project VELACS—Control test results. Journal of geotechnical engineering, 119(8), 1276-1292.

Barrero, A. R., Taiebat, M., & Dafalias, Y. F. (2020). Modeling cyclic shearing of sands in the semifluidized state. International Journal for Numerical and Analytical Methods in Geomechanics, 44(3), 371-388.

Biot, M. A. (1955). Theory of elasticity and consolidation for a porous anisotropic solid. Journal of applied physics, 26(2), 182-185.

Boulanger, R. W. (2003) High overburden stress effects in liquefaction analyses. *Journal of geotechnical and geoenvironmental engineering*, ASCE, 129(12), 1071-1082.

Boulanger, R. W., and Idriss, I. M. (2004) State normalization of penetration resistance and the effect of overburden stress on liquefaction resistance. *Proceedings 11th SDEE and 3rd ICEGE*, University of California, Berkeley, CA.

Boulanger, R. W., & Ziotopoulou, K. (2013). Formulation of a sand plasticity plane-strain model for earthquake engineering applications. Soil Dynamics and Earthquake Engineering, 53, 254-267.

Boulanger, R. W., & Idriss, I. M. (2014) CPT and SPT based liquefaction triggering procedures. Report No. UCD/CGM.-14, 1.

Cheng, Z. (2018) A practical 3D bounding surface plastic sand model for geotechnical earthquake engineering application. In Geotechnical Earthquake Engineering and Soil Dynamics V: Numerical Modeling and Soil Structure Interaction (pp. 37-47). Reston, VA: American Society of Civil Engineers.

Cheng, Z., Detournay, C. (2021) Formulation, validation and application of a practice-oriented two-surface plasticity sand model. *Computers and Geotechnics,* 132, https://doi.org/10.1016/j.compgeo.2020.103984.

Dafalias, Y.F. and Manzari, M.T. (2004) Simple plasticity sand model accounting for fabric change effects. Journal of Engineering Mechanics, 130(6), pp. 622-634.

Dashti, S., Bray, J. D., Pestana, J. M., Riemer, M., & Wilson, D. (2010). Mechanisms of seismically induced settlement of buildings with shallow foundations on liquefiable soil. Journal of geotechnical and geoenvironmental engineering, 136(1), 151-164.

Dobry, R. and Abdoun, T. (2015) Cyclic shear strain needed for liquefaction triggering and assessment of overburden pressure factor K_σ. J. Geotech. Geoenviron. Eng., 10.1061/(ASCE)GT.1943-5606.0001342, 04015047.

Elgamal, A. W., Zeghal, M., Tang, H. T., and Stepp, J. C. (1995) Lotung downhole array. I: evaluation of site dynamic properties. Journal of geotechnical and geoenvironmental engineering, ASCE, 121(4), 350-362.

Elgamal A., Yang Z., Parra E. and Ragheb A. (2003) Modeling of cyclic mobility in saturated cohesionless soils. *Int. J. Plasticity,* 19, (6), 883-905.

El Ghoraiby, M.A., Park, H., and Manzari, M.T. (2017). LEAP 2017: soil characterization and element tests for Ottawa F65 sand. The George Washington University, Washington, DC.

Gerolymos, N., and Gazetas, G. (2005) Constitutive model for 1-D cyclic soil behavior applied to seismic analysis of layered deposits. *Soils and Foundation*, 45(3), 147-159.

Gillette, D. (2021) US Bureau of Reclamation, Personal communication .

Hashash, Y. M. A. (2009) DEEPSOIL V 3.7, Tutorial and User Manual. 2002-2009. University of Illinois at Urbana-Champaign, Urbana, Illinois.

Hynes, M. E., Olsen, R. S., and Yule, D. E. (1999) Influence of confining stress on Liquefaction Resistance. *Proc., Int. Workshop on Phys. And Mech. Of Soil Liquefaction*, Balkema, Rotterdam, The Netherlands, 145–152.

Idriss, I. M., and Boulanger R. W. (2006) Semi-empirical procedures for evaluating liquefaction potential during earthquakes *Soil Dynamics and Earthquake Engineering*, 26(2-4), 115-130.

Idriss, I.M., and Boulanger, R.W. (2008) Soil liquefaction during earthquakes. *Monograph MNO-12*, Earthquake Engineering Research Institute. Oakland, CA.

Ishihara, K. (1993) Review of the predictions for Model 1 in the VELACS program. Verification of numerical procedures for the analysis of soil liquefaction problems (VELACS). Arulanandan K. and Scott R.F., editors. Rotterdam: A.A. Balkema; 1353–68.

Kayen, R., Moss, R. E. S., Thompson, E. M., et al. (2013) Shear-wave velocity–based probabilistic and deterministic assessment of seismic soil liquefaction potential. Journal of Geotechnical and Geoenvironmental Engineering, 139(3), 407-419.

Lee, M. K., and Finn, W. D. (1978) DESRA-2, Dynamic effective stress response analysis of soil deposits with energy transmitting boundary including assessment of liquefaction potential. Soil Mechanics Series, No. 36, Department of Civil Engineering, University of British Columbia, Vancouver, Canada.

LEAP-2017 GWU Laboratory Tests (2017), in LEAP-2017 GWU Laboratory Tests. DesignSafe-CI, doi:10.17603/DS2210X

Li, X., Wang, Z. L., and Shen, C. K. (1993) SUMDES. A nonlinear procedure for response analysis of horizontally layered sites subjected to multidirectional earthquake loading. Department of Civil Engineering, University of California at Davis.

Manzari, M. T., & Dafalias, Y. F. (1997) A critical state two-surface plasticity model for sands. Geotechnique, 47(2), 255-272.

Manzari, M.T., Ghoraiby, M.E., Kutter, B.L, et al. (2017) Liquefaction Experiment and Analysis Projects (LEAP): summary of observations from the planning phase. LEAP Special Issue, *Journal of Soil Dynamics and Earthquake Engineering* (in press).

McKenna, F., and Fenves, G. L. (2001) The OpenSees Command Language Manual: version 1.2." PEER Center, University of California at Berkeley.

Montgomery, J., Boulanger, R. W., and Harder, L. F., Jr. (2012) Examination of the K_σ overburden correction factor on liquefaction resistance. *Report No. UCD/CGM-12-02*, Center for Geotechnical Modeling, Department of Civil and Environmental Engineering, University of California, Davis, CA.

Ni, M., Abdoun, T., Dobry, R., Zehtab, K., Marr, A., & El-Sekelly, W. (2020) Pore pressure and K σ evaluation at high overburden pressure under field drainage conditions. I: Centrifuge experiments. Journal of Geotechnical and Geoenvironmental Engineering, 146(9), 04020088.

Prevost, J. H. (1977) Mathematical modeling of monotonic and cyclic undrained clay behavior." *International Journal of Numerical and Analytical Methods in Geomechanics*, 1(2), 195-216.

Schnabel, P. B. (1972) SHAKE: A computer program for earthquake response analysis of horizontally layered sites. EERC Report 72-12, University of California, Berkeley.

Scott, R. F. (1986) Solidification and Consolidation of a Liquefied Sand Column. Soils and Foundations, Vol. 26, No.4, 23-31, December.

Seed, R. B., and Harder Jr., L. F. (1990) SPT-based analysis of cyclic pore pressure generation and undrained residual strength. *Proc. H. Bolton Seed Memorial Symposium*, University of California, Berkeley, California.

Seed, H. B. (1983) Earthquake-resistant design of earth dams. Proc. Seismic Design of Earth Dams and Caverns, ASCE, Philadelphia, Pennsylvania, May 16-20.

Seed, H. B. (1979) Soil liquefaction and cyclic mobility evaluation for level ground during earthquakes. *Journal of the Geotechnical Engineering Division,* 105(GT2), pp. 201-255.

Seed, H.B. and Idriss, I.M. (1971) Simplified Procedure for Evaluating Soil Liquefaction Potential." *Journal of the Soil Mechanics and Foundations Division,* (97), 1249-1273.

Sharp, M. K. and Dobry, R. (2002) Sliding Block Analysis of Lateral Spreading Based on Centrifuge Results," Intl. Journal of Physical Modelling in Geotechnics, 2(22), pp. 13-32, June.

Terzaghi, K., Peck, R. B., & Mesri, G. (1996) Soil mechanics in engineering practice. John Wiley & Sons.

Vaid, Y. P., and Thomas, J. (1995) Liquefaction and postliquefaction behavior of sand." *Journal of Geotechnical Engineering*, 121(2), 163-173.

Vaid, Y. P., & Sivathayalan, S. (1996). Static and cyclic liquefaction potential of Fraser Delta sand in simple shear and triaxial tests. *Canadian Geotechnical Journal*, *33*(2), 281-289.

Wang, R., Zhang, J. M., & Wang, G. (2014). A unified plasticity model for large post-liquefaction shear deformation of sand. Computers and Geotechnics, 59, 54-66.

Youd, T. L., Idriss, I.M., Andrus, R.D., et al. (2001) Liquefaction Resistance of Soils: Summary Report from the 1996 NCEER and 1998 NCEER/NSF Workshops on Evaluation of Liquefaction Resistance of Soils. Journal of Geotechnical and Geoenvironmental Engineering, ASCE, 127(10), 817-833.

Zou, Y. X., Zhang, J. M., & Wang, R. (2020). Seismic analysis of stone column improved liquefiable ground using a plasticity model for coarse-grained soil. Computers and Geotechnics, 125, 103690.

Zeghal, M., Elgamal, A. W., Tang, H. T. and Stepp, J. C. (1995) Lotung downhole seismic array: evaluation of soil nonlinear properties." Journal of Geotechnical Engineering, ASCE, 121(4), pp. 363-378.

Table 1. Relative density, confining pressure and g-level of centrifuge models and FLAC3D simulations

Experiment	Effective overburden pressure, σ'_{v0} (atm) [(1)]	Relative Density, D_r (%)[(2)]	Measured Experimental Maximum Pore Pressure Ratio $(r_u)_{max} = (u/\sigma'_{v0})_{max}$	Numerical Simulation	Numerically Computed $(r_u)_{max}$
Test 45-1	1	45	0.80	FLAC 45-1	0.76
Test 45-6	6	45	0.76	FLAC 45-6	0.76
Test 80-1	1	80	0.92	FLAC 80-1	0.81
Test 80-6	6	80	0.60	FLAC 80-6	0.60

(1) Effective overburden pressure before shaking at mid depth of sand layer.

(2) Rounded Relative Density. The actual relative densities of 45% and 77% measured in the centrifuge tests before shaking were used in the numerical simulations.

Table 2. P2Psand model parameters used in FLAC3D simulations of stress controlled cyclic triaxial tests to generate the experimental LSC of Fig. 12.					
Parameter	Set A (Default)	Set B (Default except K_c)	Set C	Set D (used in FLAC 80-1)	Parameter description and expression for default value
relative-density-initial D_r^0	0.715	0.715	0.715	0.77	Initial relative density before loading
factor-cyclic K_c	0.1857	2	0.3	0.32	Factor of cycling to adjust the rate of cyclic mobility and liquefaction. The default value is internally initialized as $K_c = 3.8 - 7.2D_r^0 + 3.0(D_r^0)^2$.
pressure-reference	101.3	101.3	101.3	101.3	Reference pressure (usually atmospheric pressure, p_{atm} = 101.3 kPa)
friction-critical ϕ_{cs}	33^0	33^0	33^0	33^0	Friction angle at critical state. The default value is 33^0.
coefficient-bounding n^b	0.0775	0.0775	0.0775	0.0775	The coefficient of bounding, used to define the bounding surface. The default value is $n^b = 0.16 - \phi_{cs}/400$.
coefficient-dilatancy n^d	0.465	0.465	1	1	The coefficient of dilatancy, used to define dilation surface. The default value is $n^d = 6n^b$.
critical state parameter Q	10	10	10	9	A critical state parameter used to define the shape and location of the critical state curve. The default value is 10.
critical state parameter R	1	1	1	1	A critical state parameter used to define the shape and location of the critical state curve. The default value is 1.
dilatancy-ratio-minimum K_{LB}^d	0.7	0.7	0.7	0.7	Minimum dilatancy ratio at low pressures. The default value is 0.7.
elasticity-r G_r	967.2	967.2	967.2	772	A function of relative density material parameter used to determine the elastic shear modulus, G = G_{max} as follows $G_r = 1240\ (D_r^0 + 0.01)$
fabric-maximum, z_{max}	15	15	15	15	Maximum fabric magnitude. The default value is $z_{max} = max(21D_r^{3.85}, 15)$.

factor-degradation k_d	0.21	0.21	0.21	0.19	Factor of elastic modulus degradation. The default value is $k_d = 0.46 - 0.35D_r$.
Poisson's ratio v	0.14	0.14	0.14	0.1	Poisson's ratio. The default is $v = 0.1 + 0.3v_{\phi}$, in which $0 \leq v_{\phi} = 0.015(\phi_{cs} - 25) \leq 1$.
rate-fabric, c_z	967.2	967.2	967.2	772	Rate of fabric. The default value is $c_z = G_r$
rate-plastic-shear h_0	1.7	1.7	0.5	0.4	Plastic shear rate, h_0. The default value is 1.7.
rate-plastic-volumetric A_{d0}	Internal	Internal	Internal	Internal	Plastic volumetric rate, A_{d0}. The default value is estimated internally.
ratio-reverse	0.02	0.02	0.02	0.02	Minimum change of the back-stress ratio to be considered a reverse path. The default value is 0.02.
ratio-strength, c	0.69	0.69	0.69	0.69	Strength ratio of the extension to compression triaxial strengths, c. The default value is $(3 - \sin \phi_{cs})/(3 + \sin \phi_{cs})$.
void-maximum e_{max}	0.78	0.78	0.78	0.78	Maximum void ratio. The default value is $e_{max} = 1.0$.
void-minimum e_{min}	0.51	0.51	0.51	0.51	Minimum void ratio. The default value is $e_{min} = 0.6$.

Table 3. P2Psand Set D parameters used in FLAC3D simulations of centrifuge tests.

Parameter	FLAC 45-1	FLAC 45-6	FLAC 80-1	FLAC 80-6
relative-density-initial D_r^0	0.45		0.77	
factor-cyclic K_c	0.8		0.32	
pressure-reference	Default (101.3 kPa)			
friction-critical ϕ_{cs}	Default (33^0)			
coefficient-bounding n^b	Default (0.0775)			
coefficient-dilatancy n^d	1			
critical state parameter Q	9			
critical state parameter R	Default (1)			
dilatancy-ratio-minimum K_{LB}^d	Default (0.7)			
elasticity-r G_r	596		772	
fabric-maximum, z_{max}	Default (15)			
factor-degradation k_d	Default (0.3)		Default (0.19)	
Poisson's ratio v	0.1			
rate-fabric, c_z	596		772	
rate-plastic-shear h_0	0.4			
rate-plastic-volumetric A_{d0}	Default (Estimated Internally)			
ratio-reverse	Default (0.02)			
ratio-strength, c	Default (0.69)			
void-maximum e_{max}	0.78			
void-minimum e_{min}	0.51			

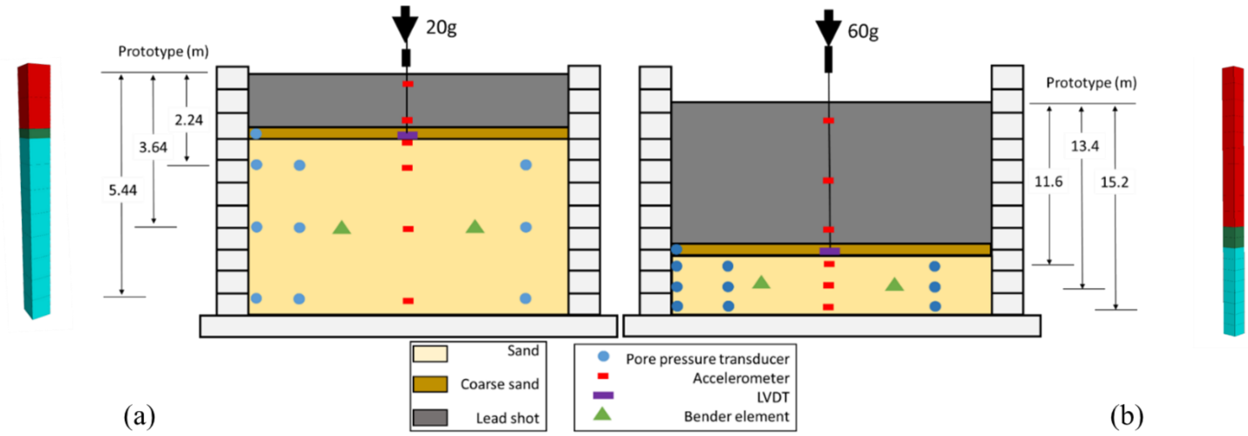

Figure 1. Physical and numerical model layout for (a) low confining pressure tests (Tests 45-1 and 80-1), and (b) high confining pressure tests (Tests 45-6 and Test 80-6)

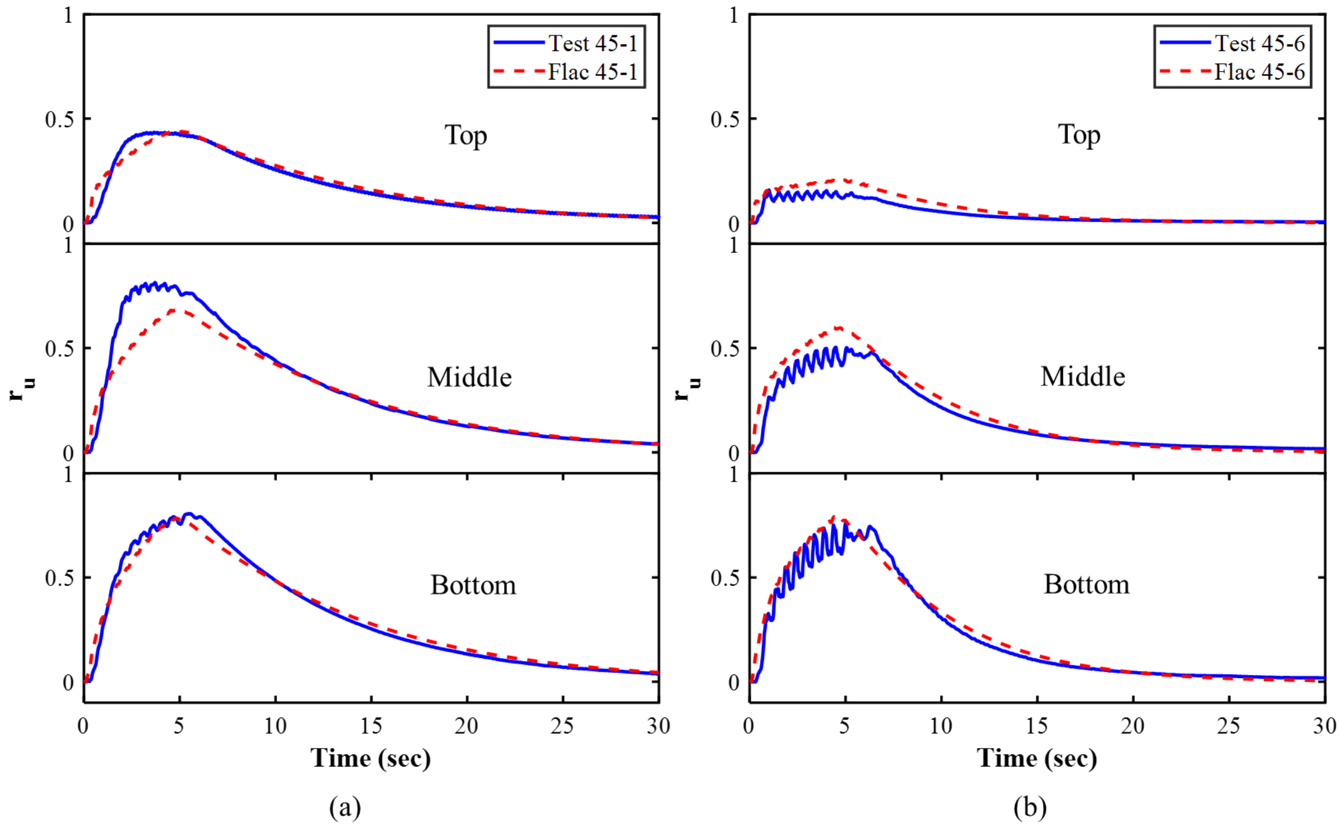

Figure 2. Experimentally recorded and numerically computed excess pore pressure ratio histories at the top, middle and bottom of the sand layer for (a) Test 45-1, and (b) Test 45-6

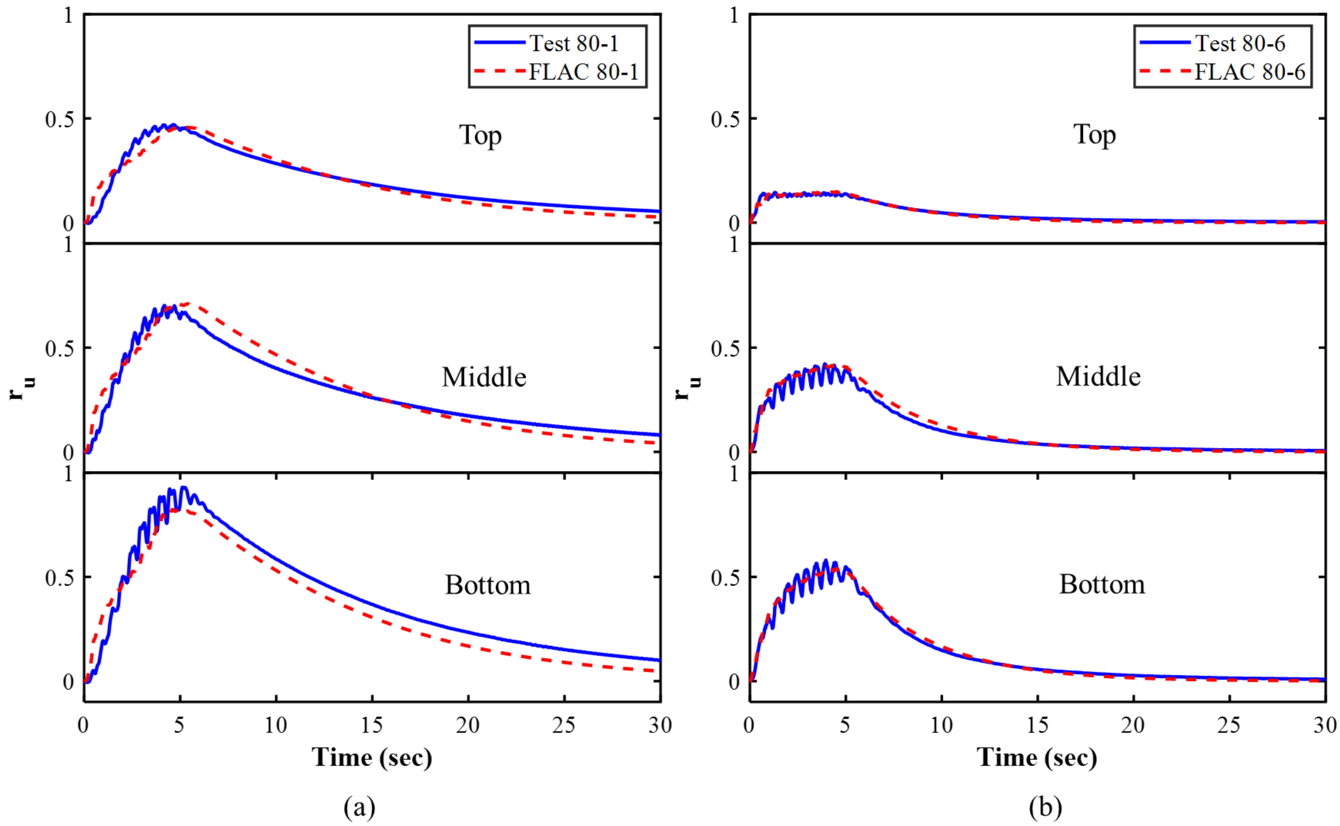

Figure 3. Experimentally recorded and numerically computed excess pore pressure ratio histories at the top, middle and bottom of the sand layer for (a) Test 80-1, and (b) Test 80-6

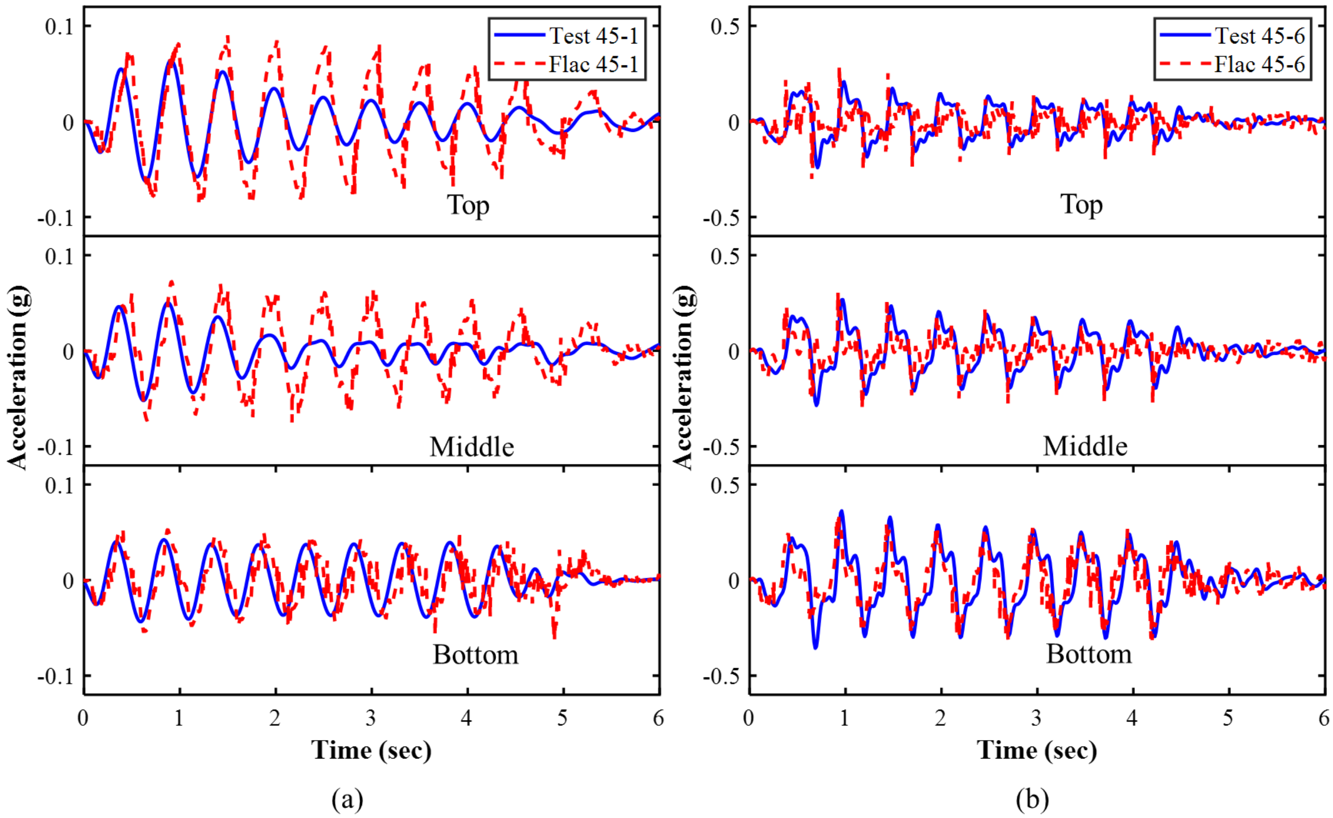

Figure 4. Experimentally recorded and numerically computed acceleration histories at the top, middle and bottom of the sand layer for (a) Test 45-1, and (b) Test 45-6

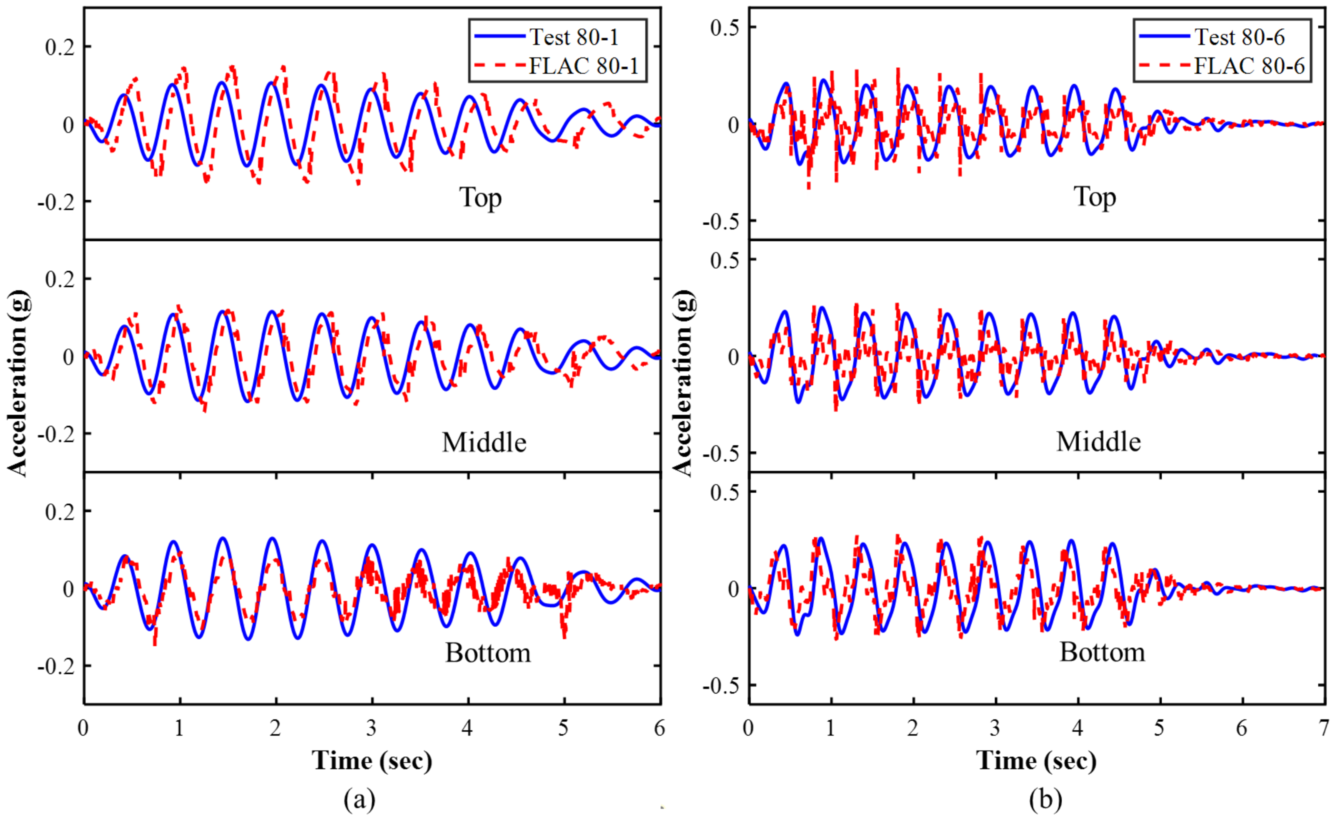

Figure 5. Experimentally recorded and numerically computed acceleration histories at the top, middle and bottom of the sand layer for (a) Test 80-1, and (b) Test 80-6

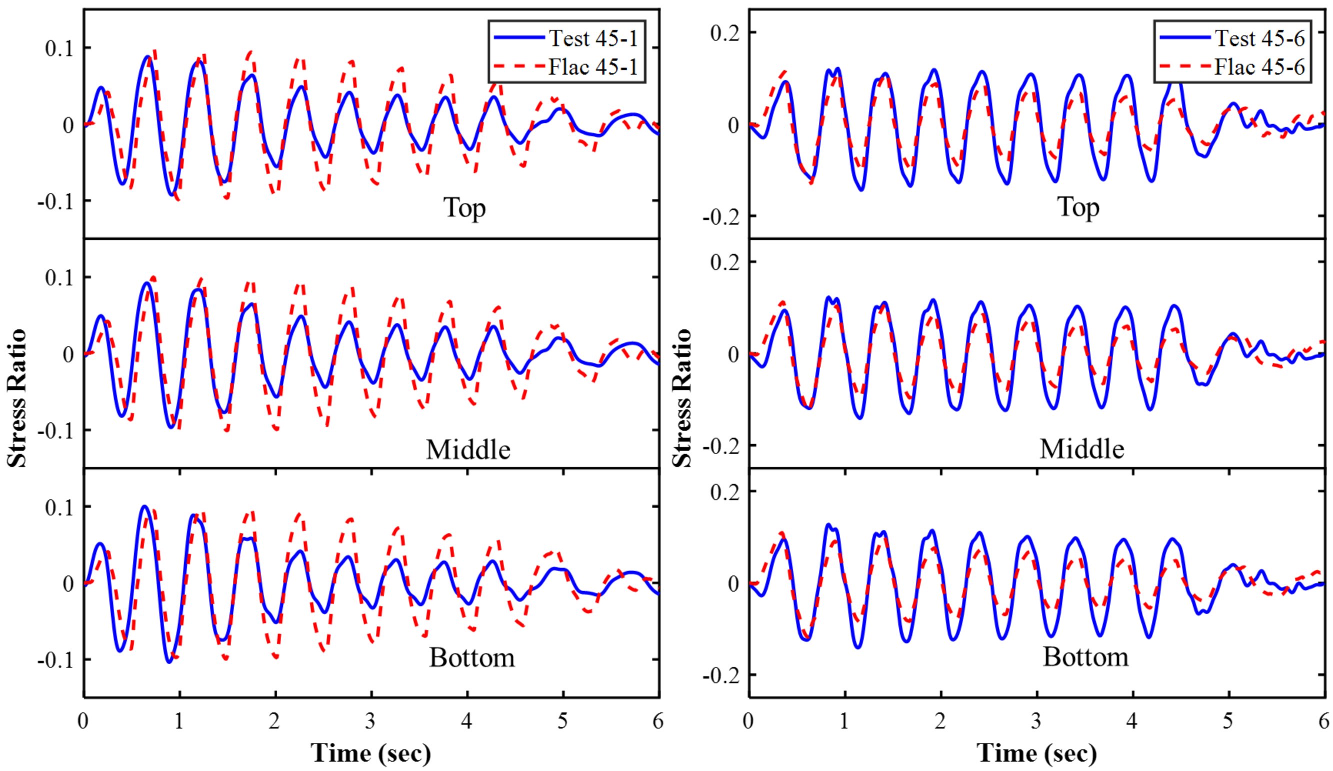

(a) (b)

Figure 6. Experimentally and numerically computed shear stress ratio histories at the top, middle and bottom of the sand layer for (a) Test 45-1, and (b) Test 45-6

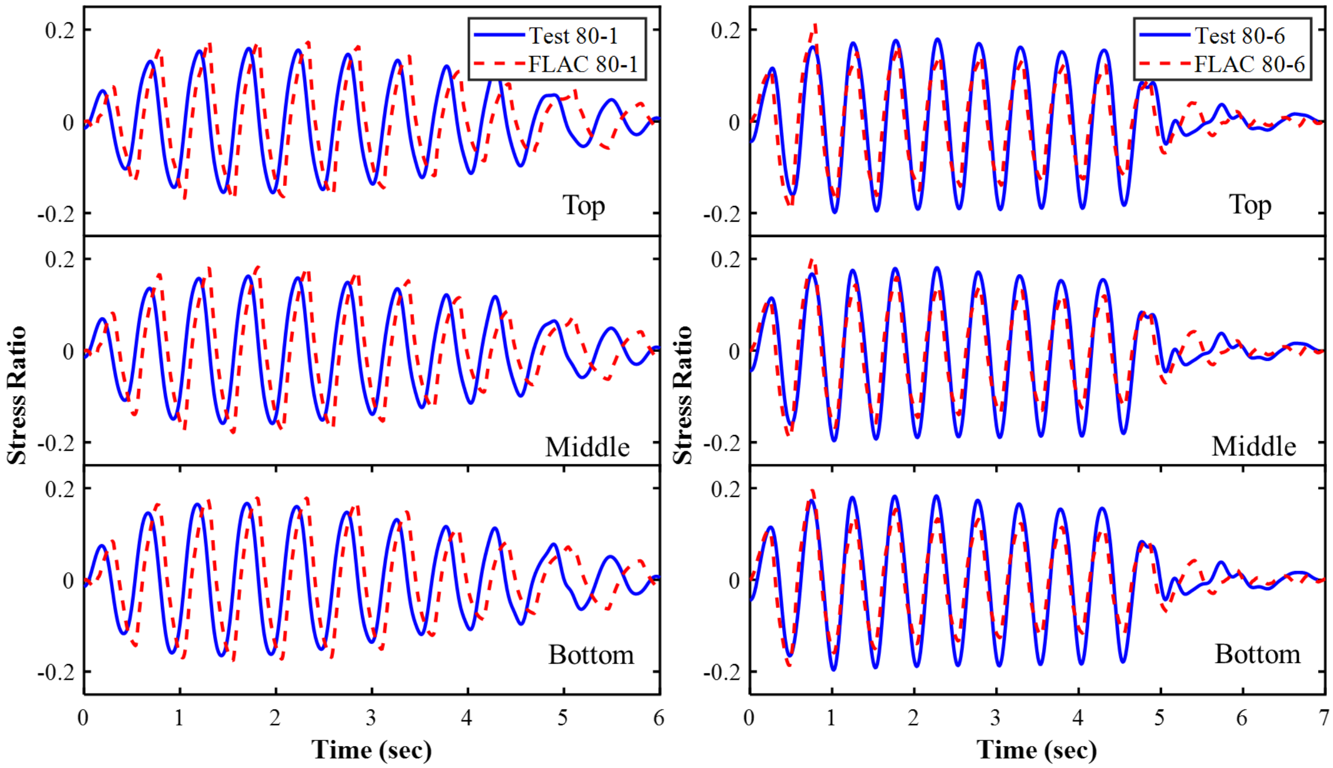

(a) (b)

Figure 7. Experimentally and numerically computed shear stress ratio histories at the top, middle and bottom of the sand layer for (a) Test 80-1, and (b) Tests 80-6

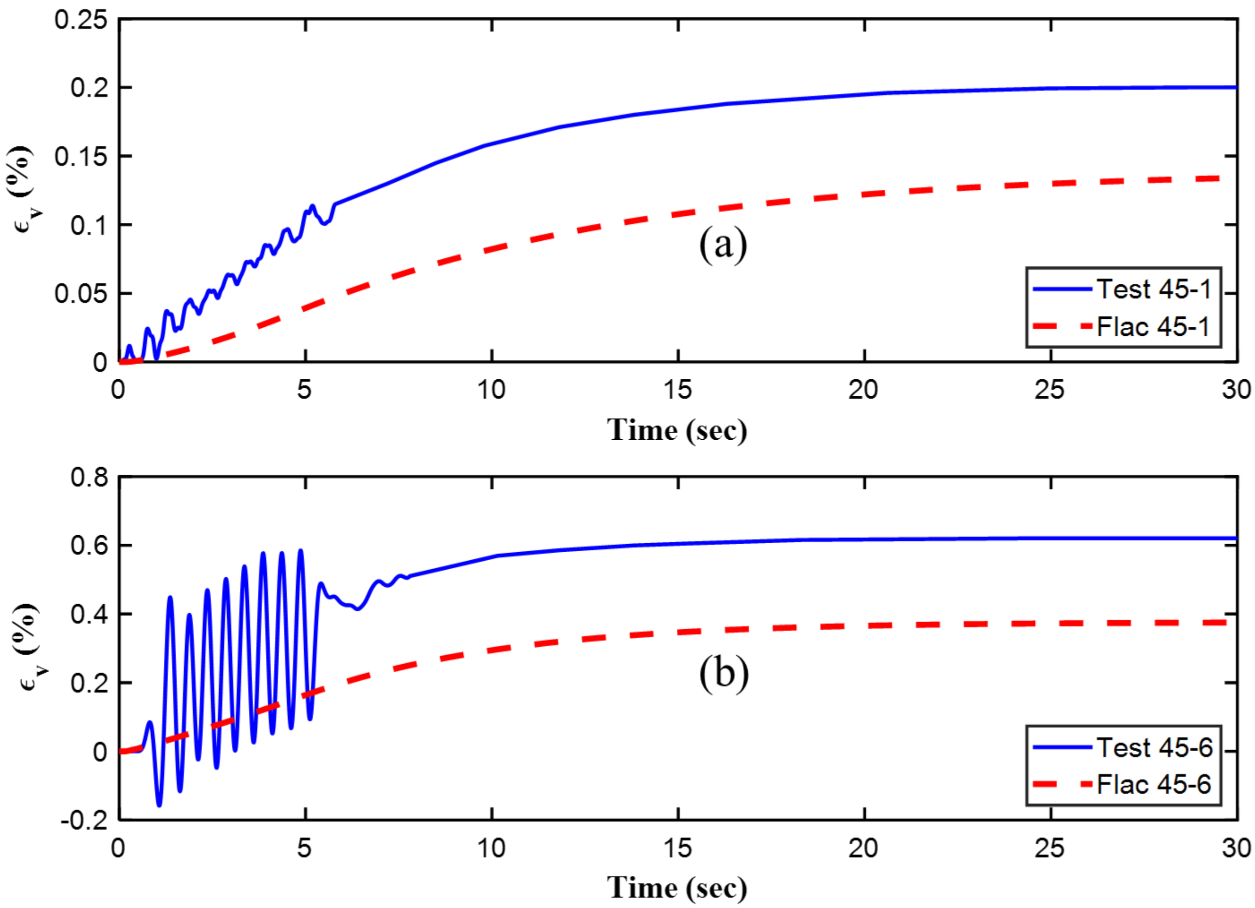

Figure 8. Experimentally and numerically computed total vertical strain histories of the sand layer for (a) Test 45-1, and (b) Test 45-6

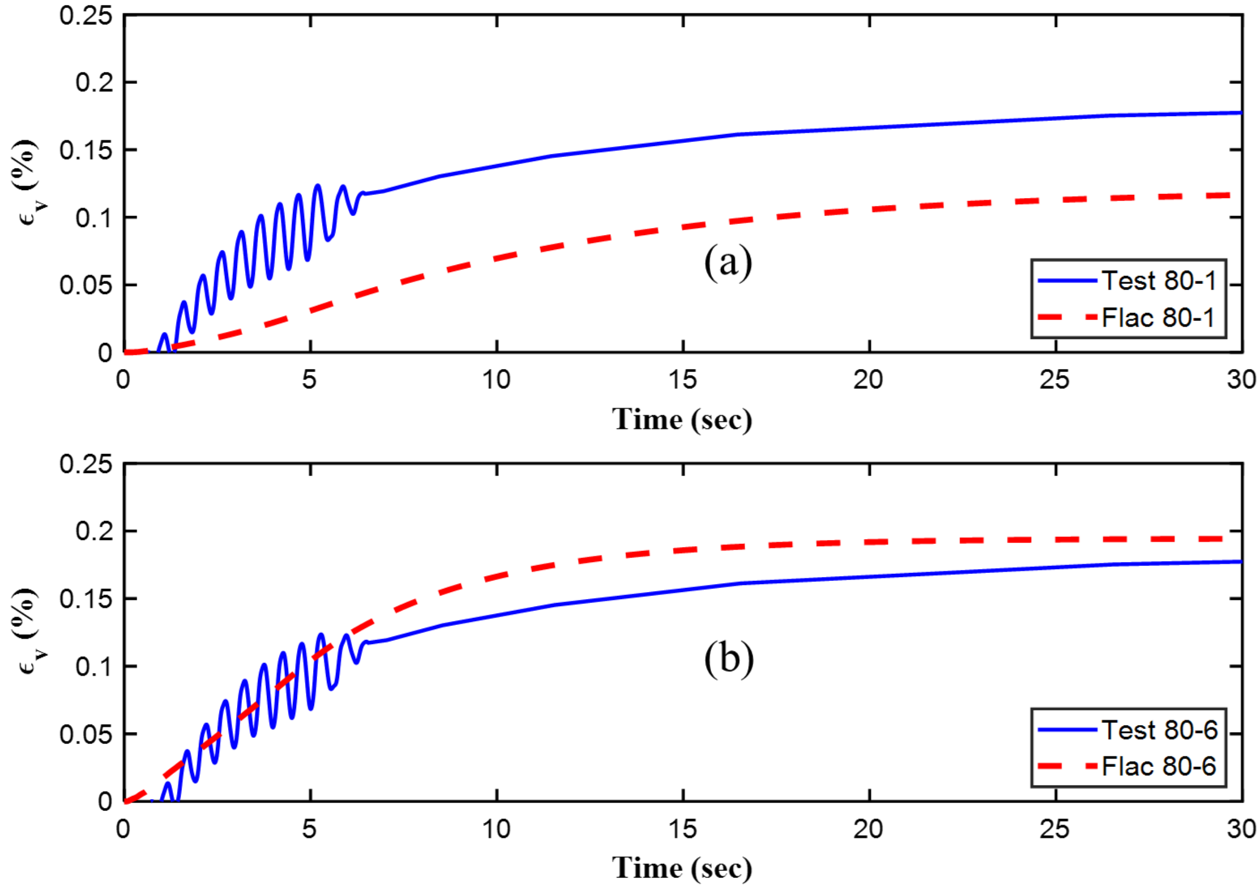

Figure 9. Experimentally and numerically computed total vertical strain history of the sand layer for (a) Test 80-1, and (b) Test 80-6

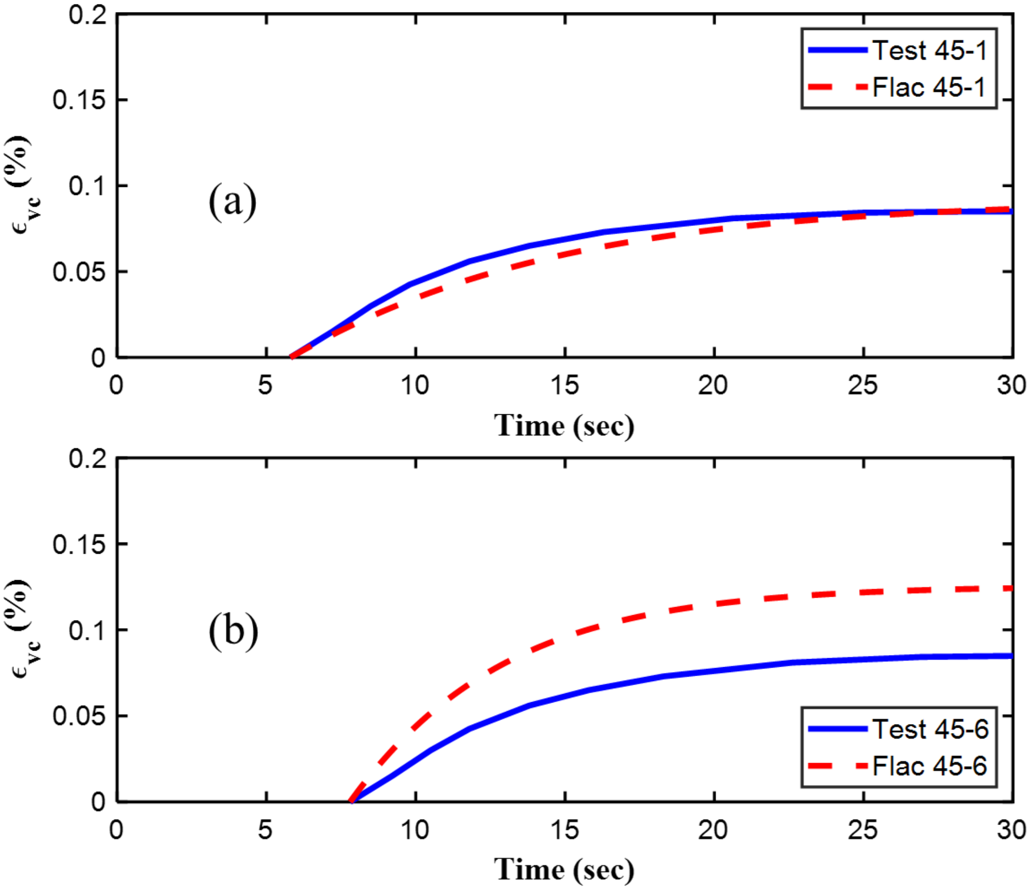

Figure 10. Experimentally and numerically computed vertical strain histories of the sand layer after the end of shaking for (a) Tests 45-1, and (b) Tests 45-6

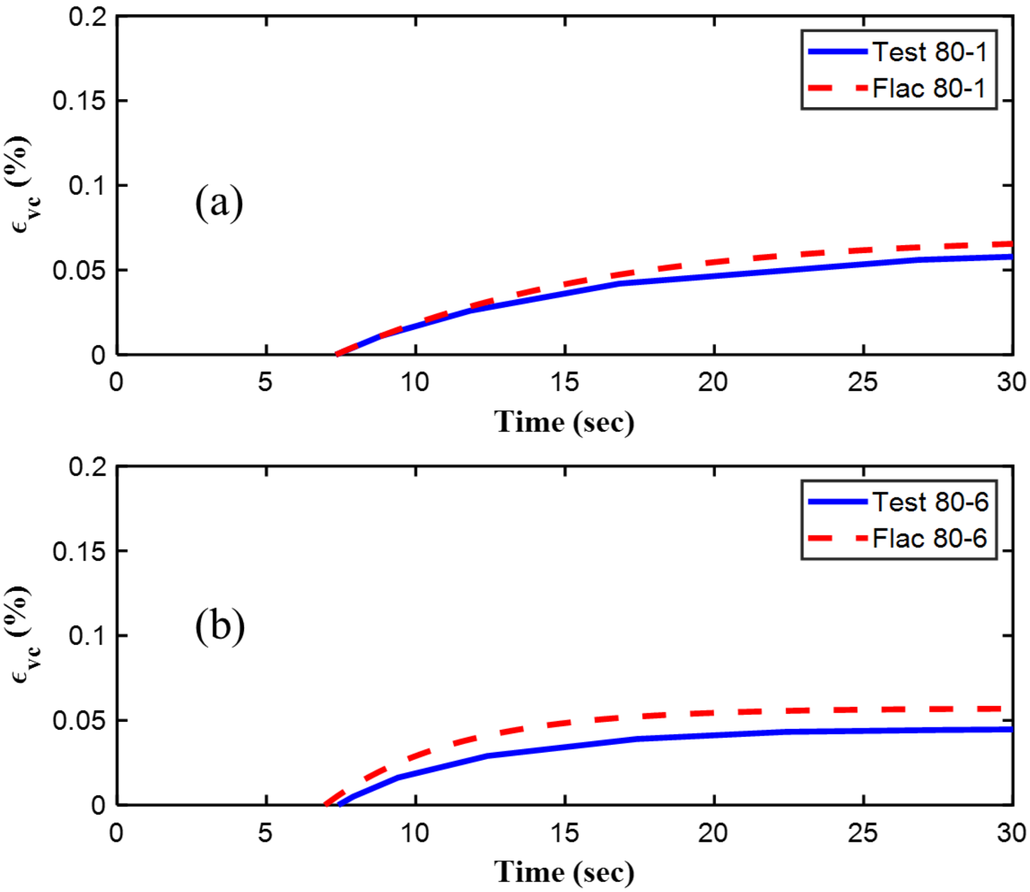

Figure 11. Experimentally and numerically computed vertical strain histories of the sand layer after the end of shaking for (a) Tests 80-1, and (b) Tests 80-6

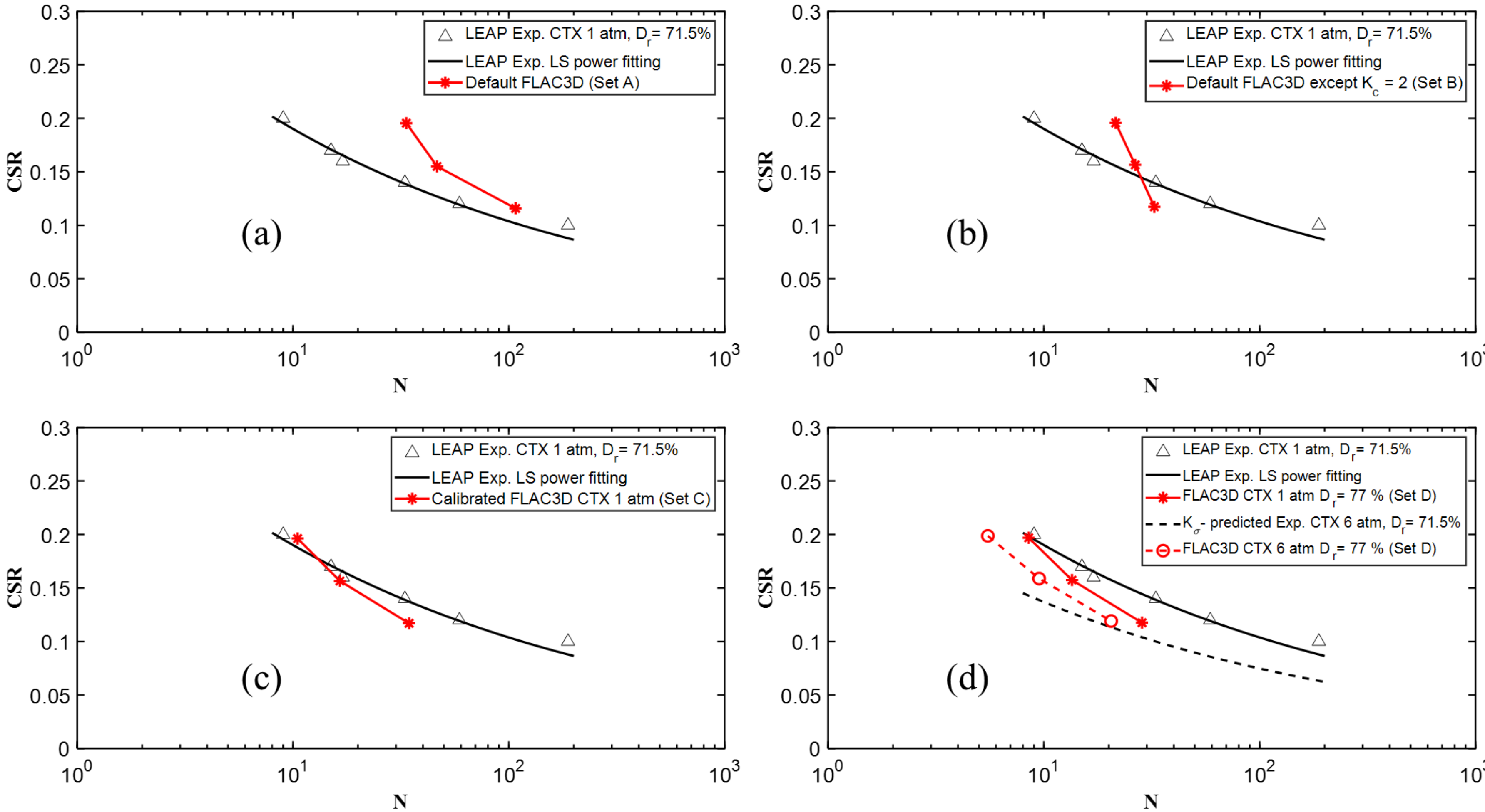

Figure 12. Cyclic stress ratio (CSR) versus number of cycles (N) required to reach a single amplitude vertical strain of 2.5% (liquefaction strength curves, LSC) of LEAP cyclic stress-controlled triaxial experiments and Flac3D numerical simulations using P2Psand model parameter sets from Table 2: a) Set A, b) Set B, c) Set C, and d) Set D .

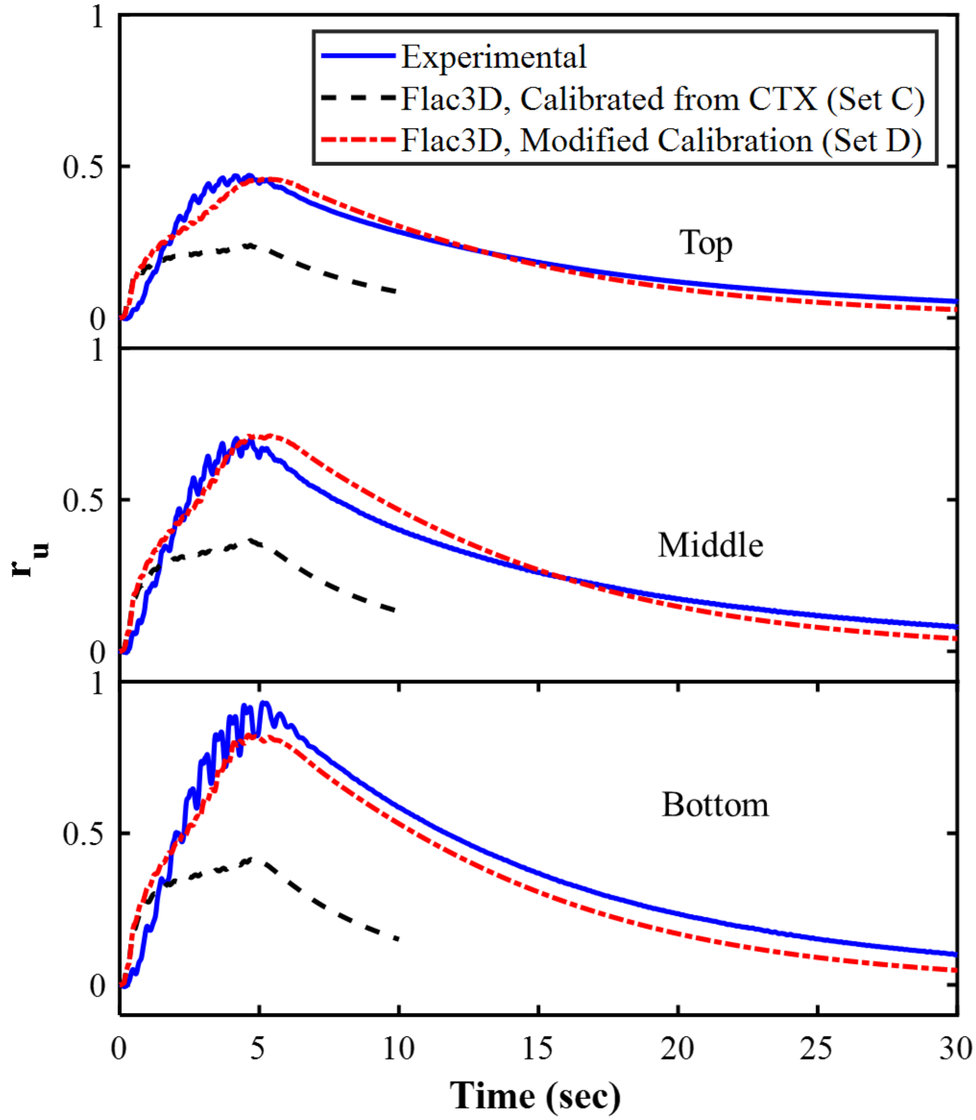

790

791 Figure 13. Experimentally recorded and numerically computed excess pore pressure ratio histories at
792 the top, middle and bottom of the sand layer for Test 80-1, using parameter Sets C and D from Table 2

793

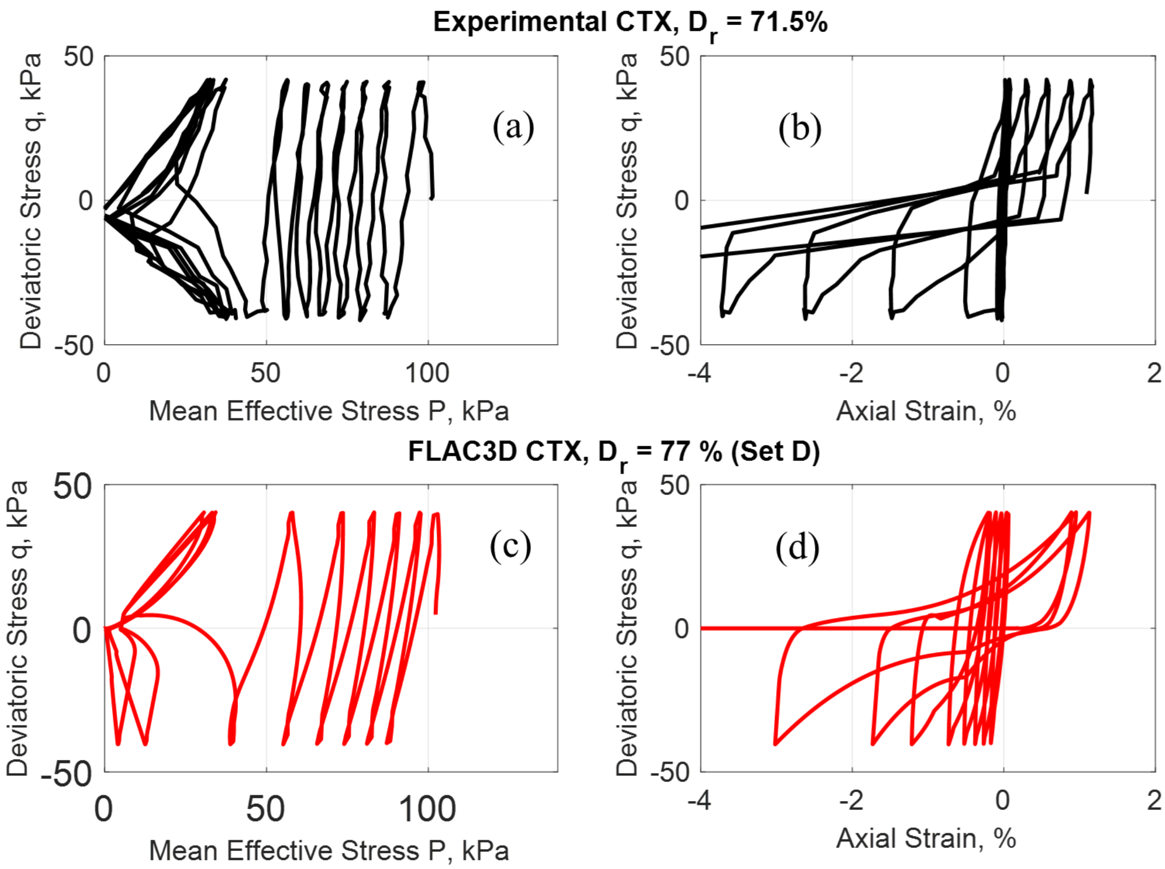

Figure 14. Stress paths and stress-strain loops of cyclic triaxial test on Ottawa F65 sand, D_r = 71.5%, consolidation pressure = 100 kPa, CSR = 0.2, and number of cycles ~ 10 cycles reported by LEAP : a) CTX experimental stress path, b) CTX experimental stress-strain loops, c) CTX FLAC3D simulated stress path using P2P and Set D parameters, and d) CTX FLAC3D simulated stress-strain loops using P2P and Set D parameters

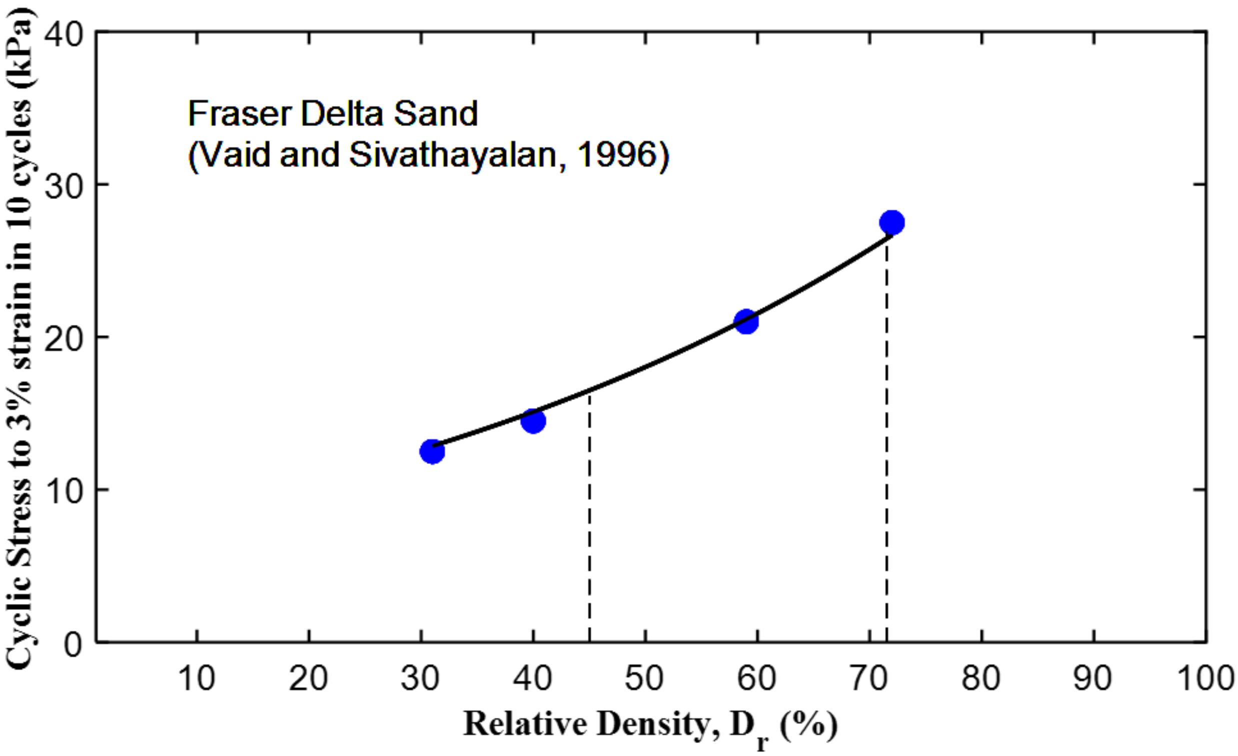

Figure 15. Cyclic stress-controlled triaxial test results for clean Fraser Delta sand, showing the cyclic stresses that cause 3% shear strain in 10 uniform cycles at relative densities of 31–72% and an effective consolidation stress of 100 kPa (data from Vaid and Sivathayalan 1996 and Idriss and Boulanger 2008).

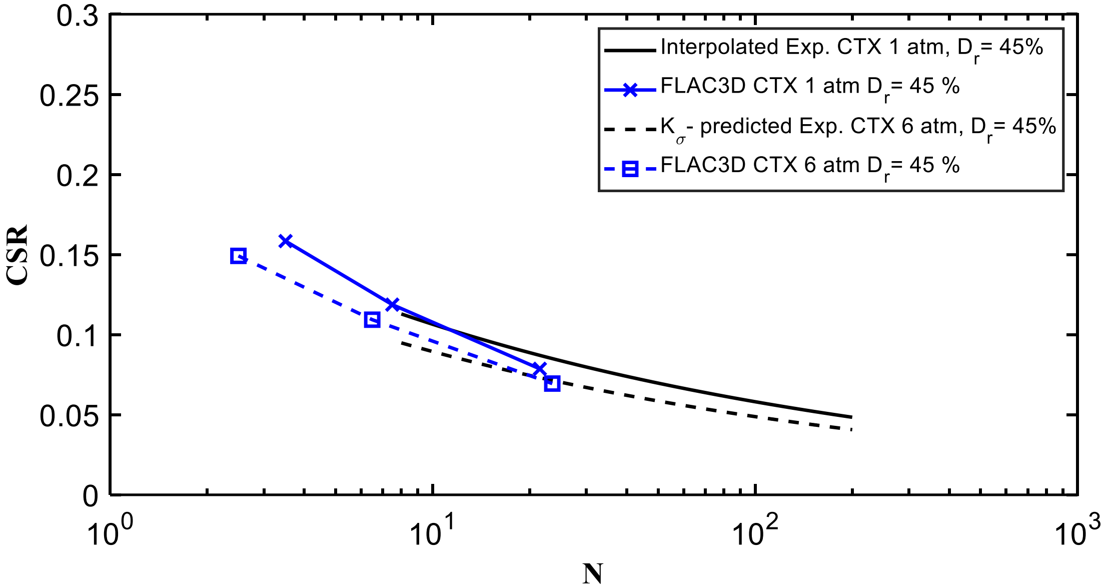

Figure 16. Cyclic stress ratio (CSR) versus number of cycles (N) required to reach a single amplitude vertical strain of 2.5% (aka liquefaction strength curves, LSC) of cyclic stress-controlled triaxial experiments and Flac3D numerical simulations using parameters from Table 3, D_r = 45%

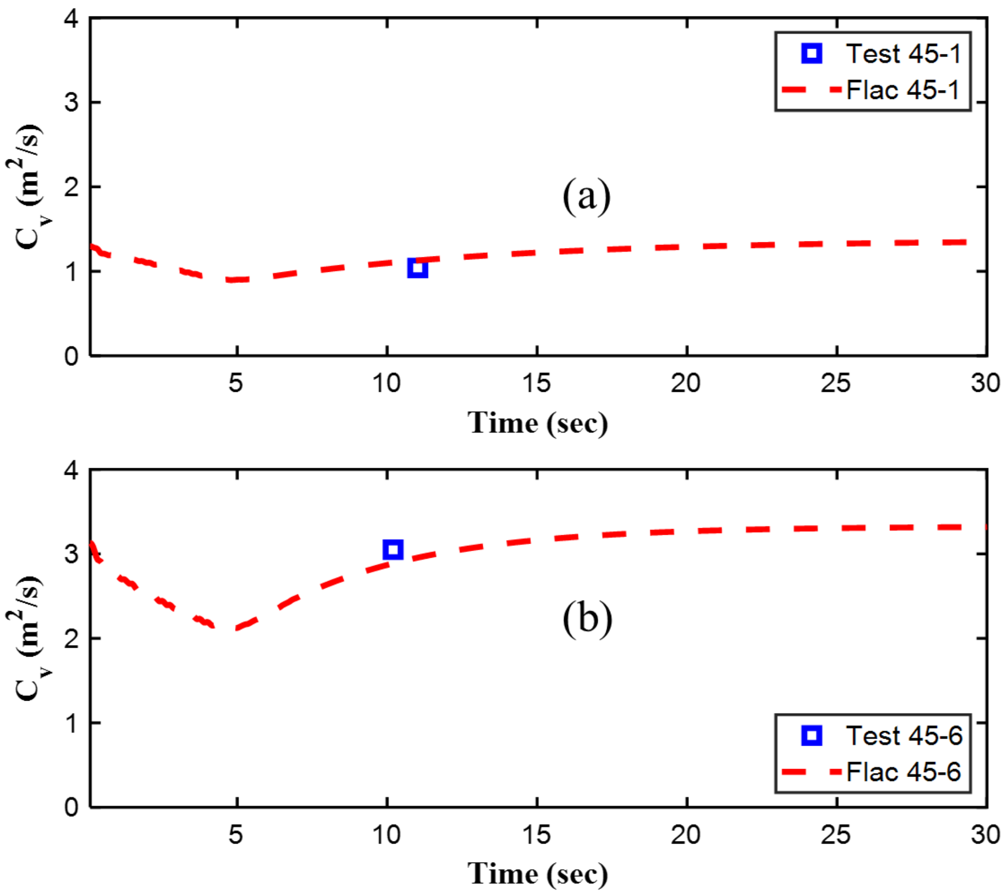

Figure 17. Experimentally and numerically computed average diffusivity of the sand layer after the end of shaking for (a) Test 45-1, and (b) Test 45-6

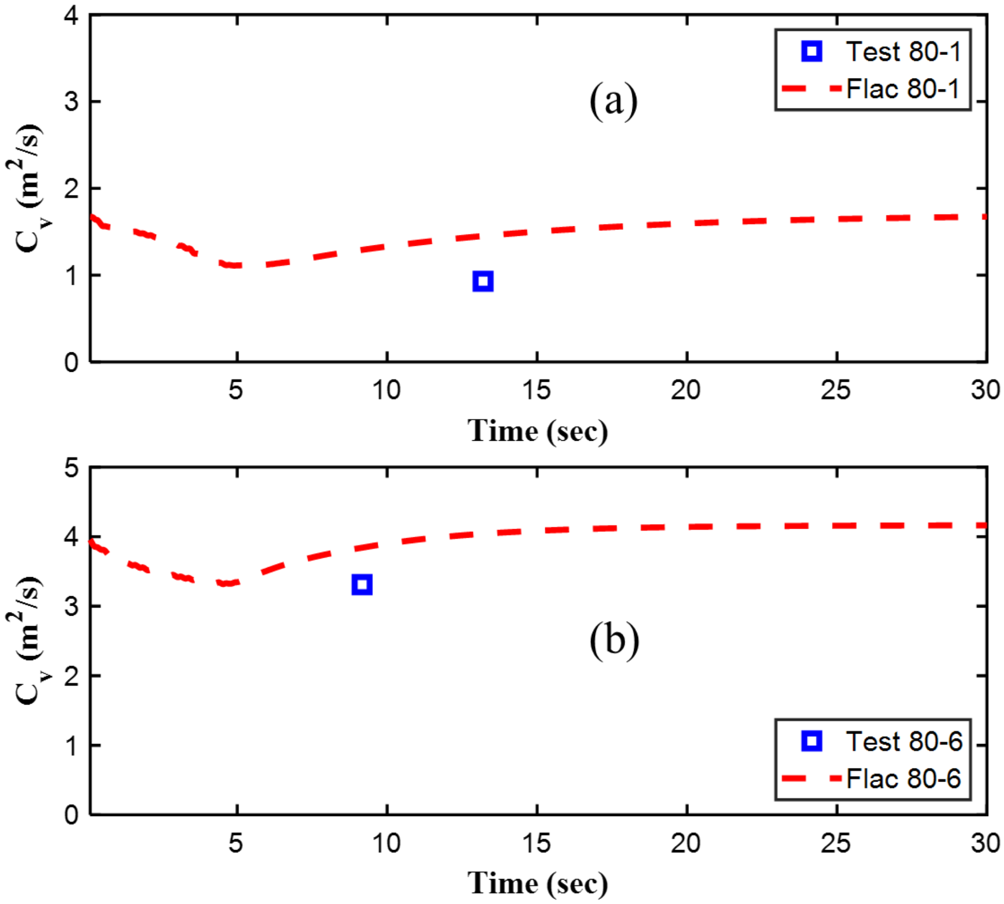

Figure 18. Experimentally and numerically computed average diffusivity of the sand layer after the end of shaking for (a) Test 80-1, and (b) Test 80-6

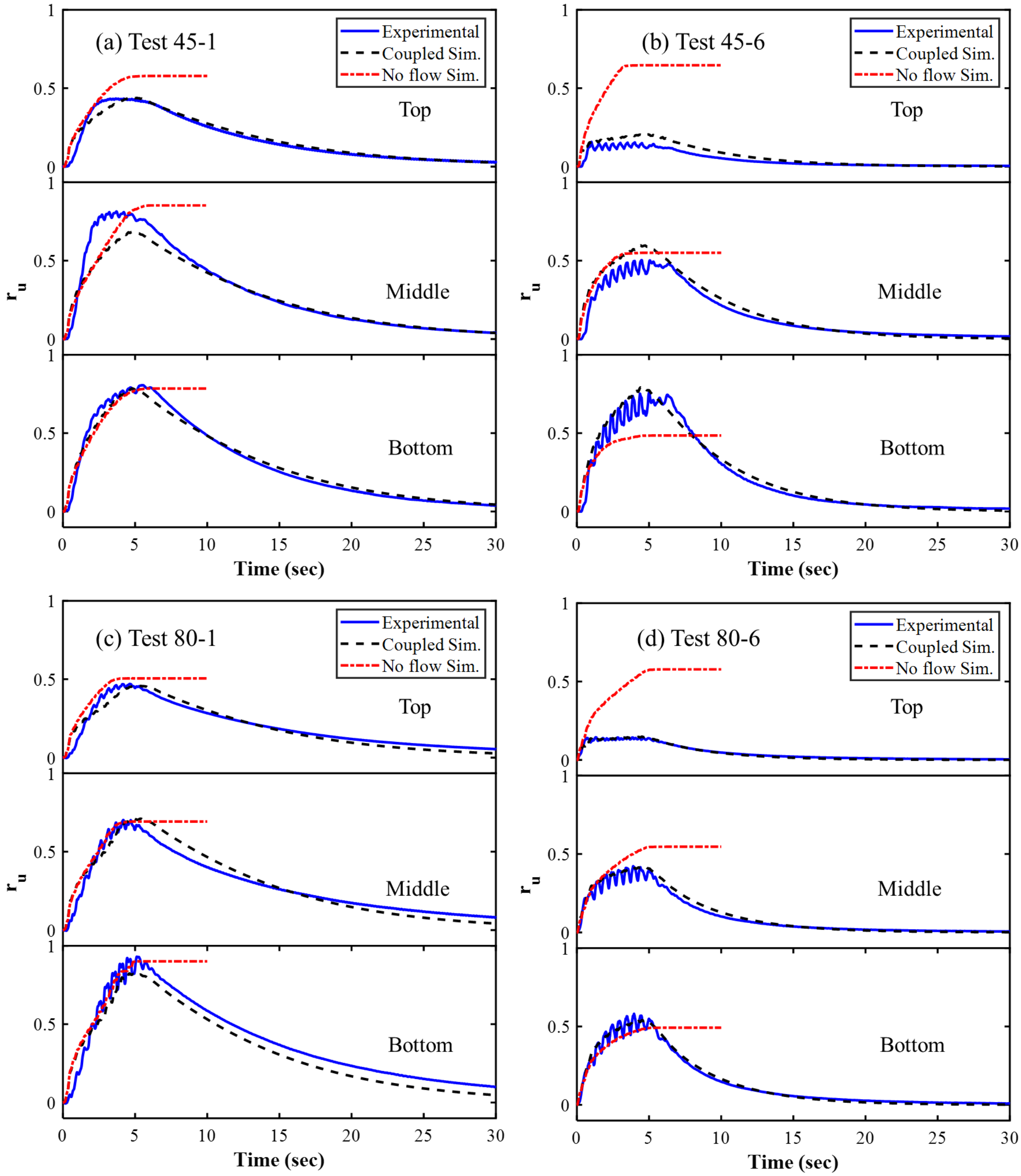

Figure 19. Experimentally recorded and numerically computed excess pore pressure ratio histories for fully coupled and no flow analyses at the top, middle and bottom of the sand layer for (a) Test 45-1, (b) Test 45-6, (c) Test 80-1, and (d) Test 80-6

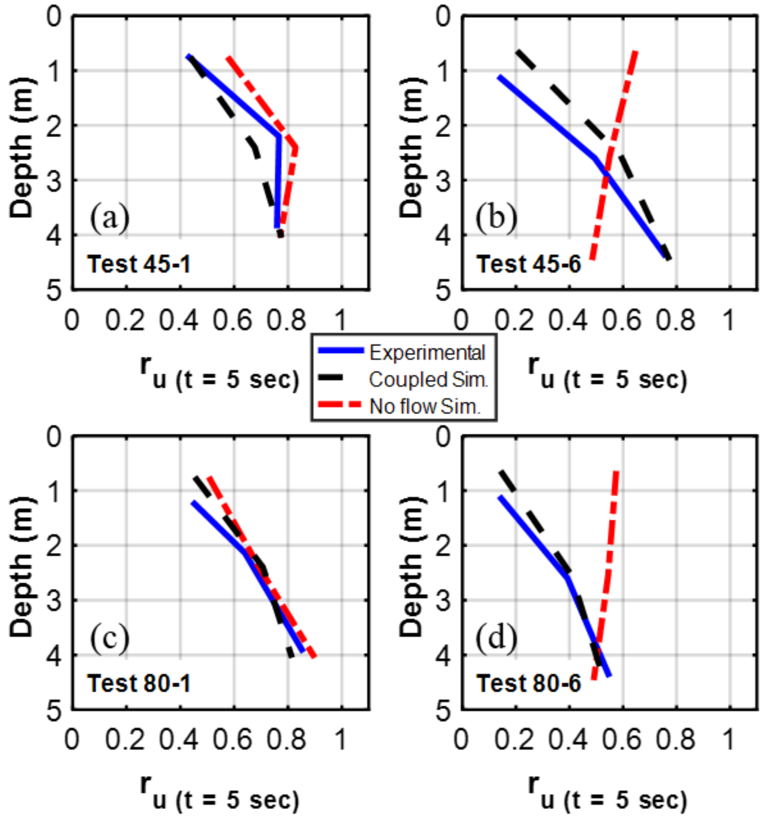

Figure 20. Experimentally recorded and numerically computed excess pore pressure ratio profiles at the end of shaking (5 sec), for fully coupled and no flow analyses for (a) Test 45-1, (b) Test 45-6, (c) Test 80-1, and (d) Test 80-6